EVALUATION OF NEAR SURFACE MATERIAL DEGRADATION IN CONCRETE USING NONLINEAR RAYLEIGH SURFACE WAVES

A Thesis
Presented to
The Academic Faculty

by

Johann Gross

In Partial Fulfillment
of the Requirements for the Degree
Master of Science in Engineering Science and Mechanics in the
School of Civil and Environmental Engineering

Georgia Institute of Technology
December 2012

EVALUATION OF NEAR SURFACE MATERIAL DEGRADATION IN CONCRETE USING NONLINEAR RAYLEIGH SURFACE WAVES

Approved by:

Professor Laurence J. Jacobs, Advisor
School of Civil and Environmental Engineering
Georgia Institute of Technology

Dr. Jin-Yeon Kim
School of Civil and Environmental Engineering
Georgia Institute of Technology

Professor Kimberly Kurtis
School of Civil and Environmental Engineering
Georgia Institute of Technology

Date Approved: 23 August 2012

ACKNOWLEDGEMENTS

The fantastic time I have had at the Georgia Institute of Technology would not have been possible without the support of people who have shown me encouragement throughout the year.

Primarily, I would like to extend my thanks to Professor Laurence J. Jacobs, who has enabled me to come to Atlanta. This work would not have been possible without his continual motivation and support in every manner. His engagement in the exchange program which I have taken part of has broadened my vision and enriched my experience in engineering science.

For sharing his expertise and extensive knowledge, providing the most insightful advice and ongoing inspiration, I am deeply grateful to Dr. Jin-Yeon Kim. Moreover, I truly thank Professor Kimberly Kurtis for supporting and advising me in specimen preparation and serving on my thesis committee. I am sincerely indebted to Professor Dr. Ing. Lothar Gaul and the Institut für Angewandte und Experimentelle Mechanik for establishing this exchange program and being the catalyst for my stay in the USA. The generous financial and organizational support provided by DAAD (German Academic Exchange Service) is greatly appreciated.

For the professional advice I have received I express my gratitude to my laboratory colleagues Katie Matlack and Chi-Won In.

I thank my companions, Christian Swacek and Daniel Zeitvogel, with whom the conversations have brightened the dreariest days. Over the year, they have become good colleagues and most of all, dear friends.

And last but not least, my most heartfelt gratitude goes to my family and to Nicola Duttle, without whose love and support I would not have been able to take and accomplish this challenge. All my friends who have contributed to making my stay in Atlanta an unforgettable experience, thank you for the friendship and memories.

TABLE OF CONTENTS

LIST OF TABLES

LIST OF FIGURES

LIST OF SYMBOLS

Symbol	Description
t_j	traction
ρ	mass density
b_j	body force
n_i	normal vector
u_i	dispacement component
σ_{ij}	second order stress tensor
C_{ijkl}	forth order stiffness tensor
ϵ_{ij}	second order strain tensor
λ and μ	Lamé's elastic constants
δ_{ij}	Kronecker Delta
∇	Differential Operator
ϕ	scalar potential
$\boldsymbol{\psi}$	vector potential
c_P	phase velocity of longitudinal wave
c_S	phase velocity of shear wave
E	Young's modulus
$\mathbf{p}$	propagation direction vector
$\mathbf{d}$	direction of particle motion
i	imaginary unit
k	wave number
ω	circular frequency
x	propagation distance
A	amplitude
θ	angle of incident, reflected and refracted waves

Symbol	Description
Λ_1 and Γ_1	constants
ν	Poisson's ratio
β	nonlinearity parameter
A_1, S_1, S_2	fundamental amplitudes
A_2	second harmonic amplitude
S_{mod}	difference component amplitude
q	amplitude modulation index
f	frequency
ϕ	phase shift
h_f	frequency modulation index
c_R	Rayleigh wave speed
d_f	far-field distance
D	diameter
λ	wave length

SUMMARY

All concrete structures are affected by carbonation. Nonlinear ultrasonic techniques are known to be sensitive to early stage damage of materials. However, only a limited number of field applicable techniques exist for damage evaluation of concrete. The objective of this research is to develop a technique that can measure the nonlinearity of concrete by using Rayleigh waves. In this work, two techniques are discussed and tested on concrete samples. The most promising method of wave mixing is found to be robust and is applied to a partly carbonated and a reference undamaged sample. The difference component of the two fundamental frequencies is used to measure the relative nonlinearity for both samples. The results show that the measured nonlinearity increases for the carbonated specimen.

CHAPTER I

INTRODUCTION

1.1 Motivation

Concrete structures are constantly exposed to environmental affects, which can cause a degradation of the material and lead to a fatal breakdown. Usually these degradation mechanisms start from the surface of the structure. One of the most prevalent environmental damages is caused by carbonation of concrete. Carbonation is a degradation mechanism that affects all outdoor, indoor and also marine-exposed structures. Air carbon dioxide penetrates the material through its natural porous network and its dissolution and the re-precipitation of calcium hydrates initiate a chemical reaction that changes the natural pH-value of the concrete. The lower pH-value destroys the passive coating of steel reinforcement bars and starts the corrosion process, which can lead to the structural failure.

Detection of the carbonation depth in a concrete the structure can prevent serious damage. A number of different nondestructive ultrasonic techniques have been used for concrete materials and have been shown to be very sensitive to microscale damage. Nonlinear impact resonance acoustic spectroscopy (NIRAS) technique for the characterization of progressive damage in standard concrete specimens was successfully applied by Leśnicki et. al [21]. It is shown in this research that microstructural changes such as crack formation and debonding between separate phases in concrete are responsible for changes in the nonlinear parameter. Also this technique could be applied to accurately classify aggregate reactivity. Damage due to thermal shock and dynamic cyclic loading was investigated by Schurr et. al [29] using Coda wave interferometry (CWI). The multiple-scattering effect of a multiphase material like concrete

allows the waves to travel through the material much longer compared to the direct path. The results are a very high sensitivity to small changes in the microstructure of the material and a creation of a diffuse ultrasonic field. The feasibility and sensitivity of this CWI-based technique in characterizing damage in cement-based materials are demonstrated. Deroo et. al [9] used diffuse ultrasound to monitor thermal damage at different stage as well as damage caused by alcali-silica reaction. For both damages a decrease in the diffusivity with increasing damage level could be measured and the results were validated by previous nonlinear ultrasound methods, which are known to be very sensitive to micro scale damage. However, this methods can only be used in the laboratory. An existing field applicable technique for metals is the second harmonic generation technique. It has the advantage of using only one side of the specimen by generating Rayleigh surface waves. Besides, it is known that Rayleigh surface waves concentrate the most of their energy very close to the surface of the material and can therefore be used to evaluate near surface damage especially well. However, only a limited amount of field applicable nondestructive ultrasonic evaluation techniques for early stage damage are known to date for concrete structures.

1.2 Objectives

The goal of this research is to develop a field applicable nondestructive ultrasonic technique for the evaluation of near surface microscale damage in concrete materials. A robust experimental procedure using Rayleigh surface waves for determining the nonlinearity of concrete samples is developed and validated on carbonated and non-carbonated samples.

1.3 Structure of the thesis

This thesis starts with a short introduction to the basic wave propagation physics followed by a discussion on the nonlinear evaluation techniques. Chapter 3 describes some of the main material properties of concrete playing a role in this work. Also

the carbonation process is discussed in this chapter in detail. Chapters 4 and 5 give an insight in the experimental setups and procedures for the two tested techniques, respectively. In Chapter 6 the results are presented and the possible future work additionally to the drawn conclusions are summarized in Chapter 7.

CHAPTER II

WAVE PROPAGATION IN SOLIDS

Before giving a discussion on the experimental method an introductory overview of the physics and mathematics of wave propagation in solid materials will be given in this chapter. The derivation of linear equations of motion will build the starting point of this discussion accompanied by some of the most important wave propagation phenomena, which will play a role in this thesis. The second half of this chapter will be dealing with wave propagation in non-linear materials giving the necessary information for understanding of the following evaluations. Furthermore the theory of the nonlinear material evaluation technique used in this work will be discussed and mathematical derivations for the measured nonlinearity parameters will be given.

2.1 Equations of motion

The derivation of the equations of motion can be started with Newton's second law. The balance of linear momentum for a body with the surface S enclosing the volume V is given by

$$\int_S t_j \,\mathrm{d}S + \int_V \rho b_j \,\mathrm{d}V = \frac{d}{dt}\int_V \rho \dot{u}_j \,\mathrm{d}V, \tag{2.1}$$

where t_j represents the traction, ρ the material mass density, b_j the body forces and u_j is the displacement with the respective time derivative $\dot{u}_j$. The linear elasticity theory defines the traction t_j on the plane represented by the normal vector n_i as

$$t_j = \sigma_{ij} n_i, \tag{2.2}$$

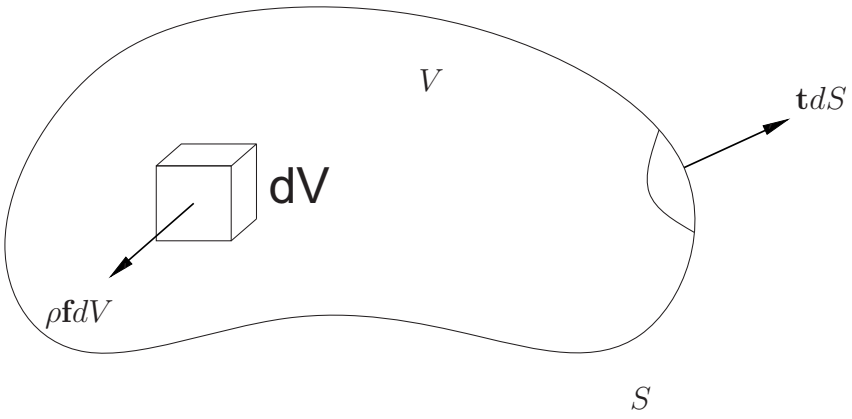

Figure 1: Balance of Momentum

where σ_{ij} denotes the second order stress tensor. By substituting Eq. (2.2) in Eq. (2.1) and applying Gauss' theorem the balance of linear momentum yields the following form:

$$\int_V (\sigma_{ij,i} + \rho b_j - \rho \ddot{u_j})\, \mathrm{d}V = 0. \tag{2.3}$$

Eq. (2.3) has to hold for every arbitrary volume, which concludes

$$(\sigma_{ij,i} + \rho b_j - \rho \ddot{u_j}) = 0. \tag{2.4}$$

This equation is known as Cauchy's equation of motion.

2.1.1 Wave propagation in linear materials

In wave propagation literature it is more common to express Cauchy's equation of motion only in terms of displacements u_i. Therefore the service of the relationship between stress and strain tensors given by

$$\sigma_{ij} = C_{ijkl}\epsilon_{kl} \tag{2.5}$$

is used. C_{ijkl} describes the forth order stiffness tensor containing the mechanical properties of the material. For the case of a linear isotropic material the constant coefficients can be expressed as

$$C_{ijkl} = \lambda \delta_{ij}\delta_{kl} + \mu(\delta_{ik}\delta_{jl} + \delta_{il}\delta_{jk}). \tag{2.6}$$

The equation contains the first order Lamé's elastic constants λ and μ. The fusion of Eq. (2.5) and Eq. (2.6) results in Hooke's law for a homogeneous, isotropic, and linear material

$$\sigma_{ij} = \lambda\epsilon_{kk}\delta ij + 2\mu\epsilon_{ij}. \tag{2.7}$$

The strain tensor ϵ_{ij} is easily formed following the relationship

$$\epsilon_{ij} = \frac{1}{2}(u_{i,j} + u_{j,i}). \tag{2.8}$$

It is reasonable to neglect the body forces in the further development. Combining Eq. (2.8) and the Hooke's law (2.7) for an isotropic, linear material Navier's equation of motion (2.9) is obtained, giving the displacement relationship

$$\mu u_{i,jj} + (\lambda + \mu)u_{j,ji} = \rho\ddot{u}_i. \tag{2.9}$$

The vector representation of Eq. (2.9) reads as

$$\mu\nabla^2\mathbf{u} + (\lambda + \mu)\nabla\nabla \cdot \boldsymbol{u} = \rho\ddot{\boldsymbol{u}}. \tag{2.10}$$

Considering the three dimensional case this equation represents a system of three coupled partial differential equations (PDEs). Usually that kind of equation system is very difficult to solve. The most common method to achieve a solution is to apply the Helmholtz decomposition (2.11), which provides two uncoupled PDEs.

$$\boldsymbol{u} = \nabla\phi + \nabla \times \boldsymbol{\psi}, \quad \nabla \cdot \boldsymbol{\psi} = 0. \tag{2.11}$$

The Helmholtz decomposition uses the gradient of the scalar potential ϕ and the curl of the zero-divergence vector potential $\boldsymbol{\psi}$. The condition of zero-divergence is necessary since three components of displacement are supposed to be described uniquely by four components of ϕ and $\boldsymbol{\psi}$. For a more detailed discussion and proof see [3]. Plugging in Eq. (2.11) into Navier's equation of motion (2.10) yields the above mentioned two PDEs:

$$\nabla^2\phi = \frac{1}{c_P^2}\ddot{\phi}, \quad \nabla^2\boldsymbol{\psi} = \frac{1}{c_S^2}\ddot{\boldsymbol{\psi}}, \tag{2.12}$$

where c_P denotes the phase velocity of the primary, or longitudinal wave, and c_S the phase velocity of the secondary, or transverse wave. Both velocities, c_P and c_S are only dependent on elastic constants and material density and are defined by

$$c_P = \sqrt{\frac{2\mu + \lambda}{\rho}}, \quad c_S = \sqrt{\frac{\mu}{\rho}}. \tag{2.13}$$

Both Lamé constants can be rewritten in respect to the material properties Young's modulus E, which is the stiffness of the material and Poisson's ratio ν, which describes the ratio between the transverse and axial strain in the applied load direction.

$$\lambda = \frac{E\nu}{(1+\nu)(1-2\nu)}, \quad \mu = \frac{E}{2(1+\nu)}. \tag{2.14}$$

2.1.2 Wave phenomena

2.1.2.1 Plane waves

For the purposes of this work it is reasonable to discuss the occurring wave phenomena under the assumption of plane waves simplifying the matters. Plane waves feature constant properties for strain $\boldsymbol{\epsilon}$, stress $\boldsymbol{\sigma}$ and displacement $\boldsymbol{u}$ in the plane perpendicular to the propagation direction $\boldsymbol{p}$. A plane displacement wave propagating with a phase velocity c can be mathematically described as

$$\boldsymbol{u} = f(\boldsymbol{x} \cdot \boldsymbol{p} - ct)\boldsymbol{d}. \tag{2.15}$$

As mentioned above $\boldsymbol{p}$ and $\boldsymbol{d}$ are unit vectors defining the directions of propagation and particle motion, respectively [3]. Using this definition in the equation of motion (2.10) yields

$$(\mu - \rho c^2)\boldsymbol{d} + (\lambda + \mu)(\boldsymbol{p} \cdot \boldsymbol{d})\boldsymbol{p} = 0. \tag{2.16}$$

Considering the fact that $\boldsymbol{d}$ and $\boldsymbol{p}$ are two different vectors the equation can be satisfied in two ways only:

$$\textit{either} \quad \boldsymbol{d} = \pm\boldsymbol{p} \quad \textit{or} \quad \boldsymbol{d} \cdot \boldsymbol{p} = 0. \tag{2.17}$$

For the first case it also can be written $\boldsymbol{d} \cdot \boldsymbol{p} = \pm 1$ and the Eq. (2.16) yields

$$c = c_P, \tag{2.18}$$

for the other case both terms in Eq. (2.16) must vanish independently and we obtain the transverse wave speed with

$$c = c_S. \tag{2.19}$$

2.1.2.2 Harmonic waves

Time harmonic plane waves play a crucial role in the present work. As a special form of plane waves propagating with the phase velocity c in the direction of the unit vector $\boldsymbol{p}$, the mathematical representation of the harmonic form can be given by

$$f(\boldsymbol{x} \cdot \boldsymbol{p} - ct) = exp[ik(\boldsymbol{x} \cdot \boldsymbol{p} - ct)]. \tag{2.20}$$

The wavenumber $k = \frac{\omega}{c} = \frac{2\pi}{\lambda}$, contained in the phase of the wave, gives the information about the quantity of wavelengths over 2π units of distance, [3]. ω is the circular frequency of the wave. Given an amplitude A, which also can be complex and is independent from $\boldsymbol{x}$ and t, we obtain an expression for a general time harmonic wave:

$$\boldsymbol{u} = Aexp[ik(\boldsymbol{x} \cdot \boldsymbol{p} - ct)]\boldsymbol{d}. \tag{2.21}$$

2.1.2.3 Joined half-spaces

One of the main phenomena that take place in the later discussed experiments occurs when waves propagate between two joined half-spaces. In a general case of in-plane motion it can be expected that for each incident wave two reflected and two refracted waves will appear in the system. A sketch of the unit propagation vectors for the system of incident a_0, reflected and refracted waves is shown in Figure 2. In the further discussion we only will focus on longitudinal waves as incident wave, since these particular ones are generated by the transducer used to excite a Rayleigh surface wave (RSW) in performed experiments. Since a RSW can be excited only when the

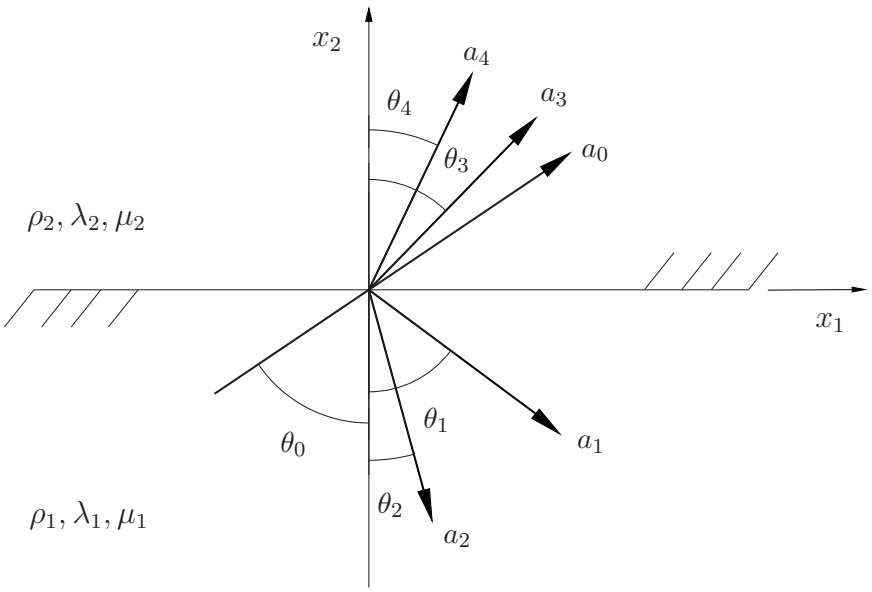

Figure 2: Incident, reflected and refracted waves

incident P-wave hits the interface of the two different materials at a particular angle a wedge was especially designed and manufactured for the purposes of this work. The angle of the wedge, and accordingly the angle of the incident wave θ_0 is only dependent on the ratio of the phase velocity of the incident wave c_{P1} and the RSW-speed in the investigated material c_{R2}.

$$\theta_0 = sin^{-1}(\frac{c_{P1}}{c_{R2}}) \tag{2.22}$$

Obviously this relationship is only defined for $c_{R2} > c_{P1}$. The mathematical derivation and proof can be found in [3].

2.1.2.4 Rayleigh surface waves

Rayleigh surface waves are named after Lord Rayleigh, who predicted their existence in 1885. One half-space like in Sec. 2.1.2.3, defined as $x_2 \leqslant 0$ shall now be considered. Rayleigh waves are able to propagate very long distances along a stress-free boundary, in positive x_1-direction, concentrating most of their energy very close to the surface. The amplitude of the Rayleigh wave decays exponentially in the negative x_2-direction. In order to describe the longitudinal and shear contributions of the Rayleigh wave

mathematically displacement potentials can be used,

$$\phi = -i\frac{\Lambda_1}{k_R} exp(-b_1 x_2) exp\left[i(k_R x_1 - \omega t)\right] \tag{2.23}$$

and

$$\boldsymbol{\psi} = -i\frac{\Gamma_1}{k_R} exp(-b_2 x_2) exp\left[i(k_R x_1 - \omega t)\right], \tag{2.24}$$

where $b_1 = \sqrt{k_R^2 - k_P^2}$ and $b_2 = \sqrt{k_R^2 - k_S^2}$, with k_R, k_P and k_S as wavenumbers of Rayleigh, primary and secondary waves. Λ_1 and Γ_1 are constants. Plugging in the Helmholtz Decomposition (2.11) into the equation of motion (2.9) and solving for displacements results in a solution of the following form:

$$u_\gamma(x_1, x_2, t) = u_\gamma^{(1)}(x_1, x_2, t) + u_\gamma^{(2)}(x_1, x_2, t). \quad \gamma = P, S. \tag{2.25}$$

The lower index γ indicates whether longitudinal or shear contribution of the total displacement. It shall be noticed that the second part on the right hand side of this equation constitutes the second order solution which will be discussed later in Section (2.2.2). Applying the boundary conditions of stress-free surface, $\sigma_{12} = \sigma_{22} = 0$ at $x_2 = 0$, to resulting equation gives the relationship for the constants Λ_1 and Γ_1 by

$$\Lambda_1 = -i\frac{2k_R b_1}{k_R^2 + b_2^2}\Gamma_1, \tag{2.26}$$

and the particular displacements for longitudinal and shear components can then be defined as

$$u_1^{(1)}(x_1, x_2, t) = \Lambda_1 \left(exp(-b_1 x_2) - \frac{2b_1 b_2}{k_R^2 + b_2^2} exp(-b_2 x_2) \right) exp\left[i(k_R x_1 - \omega t)\right], \tag{2.27}$$

$$u_2^{(1)}(x_1, x_2, t) = i\Lambda_1 \frac{b_1}{k_R} \left(exp(-b_1 x_2) - \frac{2k_R^2}{k_R^2 + b_2^2} exp(-b_2 x_2) \right) exp\left[i(k_R x_1 - \omega t)\right]. \tag{2.28}$$

For a unique first order solution at $x_2 = 0$ it is also required that the Rayleigh wave velocity c_R satisfies the following characteristic equation:

$$(2 - \frac{c_R^2}{c_S^2})^2 - 4\sqrt{\left(1 - \frac{c_R^2}{c_P^2}\right)\left(1 - \frac{c_R^2}{c_S^2}\right)} = 0, \tag{2.29}$$

It is noted that the wavenumber is not affecting the equation for the phase velocity of the Rayleigh wave (2.29), which means it does not depend on the frequency and therefore is nondispersive at free surface of an elastic half-space. Rayleigh surface waves propagate at approximately 90% of the shear wave velocity. An accredited approximation is given in [3] by

$$c_R = \frac{0.862 + 1.14\nu}{1 + \nu} c_S. \tag{2.30}$$

For this research Rayleigh waves are of an eminent importance, since near-surface degradation of concrete material shall be investigated.

2.2 Non-linear wave propagation

So far we only considered material with an ideally linear stress-strain-relationship. In heterogenous, multi-phase and damaged materials the stress-strain relationship does not follow the linear character of Hooke's law (2.7) [5]. A detailed derivation of nonlinear stress-strain relationship can also be found in [20] and the equation is given by:

$$\sigma = E\epsilon \left[1 + \beta\epsilon + \delta\epsilon^2 ...\right] + \alpha \left(\epsilon, sign\left(\dot{\epsilon}\right)\right), \tag{2.31}$$

the dotted ϵ relates to the time derivative of the strain, α is the non-classical non-linear parameter and the *sign* function equals $+1$ when $\dot{\epsilon} > 0$ and -1 when $\dot{\epsilon} < 0$. Eq. (2.31) can be used for practical estimates very well, especially for non-destructive evaluations (NDE). Furthermore, most of such materials also show non-symmetric behaviour under tensile and compressive loads. The simplest way to explain this effect is by imagining a micro-crack represented by two surfaces interacting with each other. Under exposure to a longitudinal wave these surfaces will come into direct contact during the compressional phase passes through. And while the tensile phase passes through the crack the surfaces will lose contact to each other producing a distortion in

the passing wave [33]. These distortions manifest themselves in a generation of higher harmonics in an initially monochromatic signal. In terms of visualization of this effect

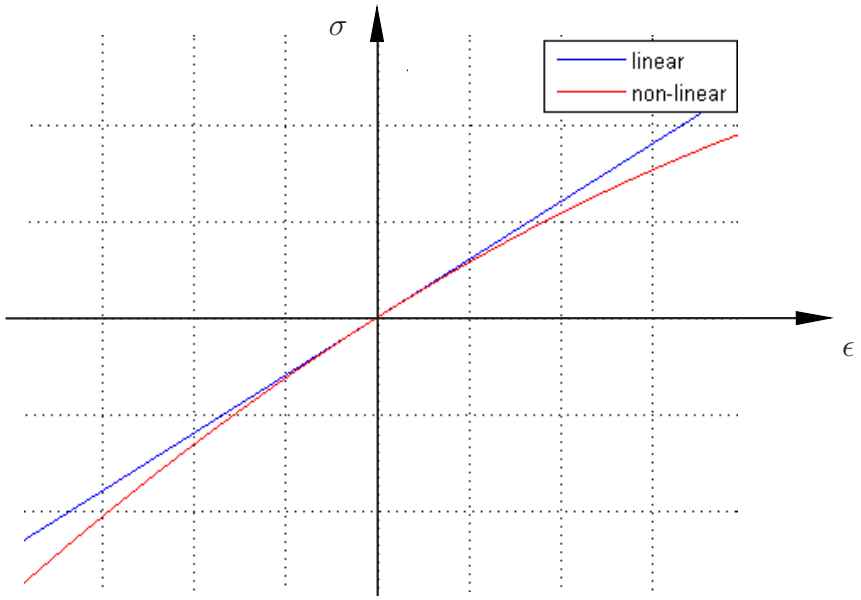

Figure 3: Comparison stress-strain relationships

the received signal can be digitally processed by software tools like MATLAB. A more detailed discussion on that process will be given in Section 4.2.3.2. In Figure 4 a very simplified example of an monochromatic input signal and an output signal with due to material non-linearity generated higher harmonics are given for a general visualization. The mathematical approach to the nonlinear wave equation has been developed in multiple works and can be found for example in [3, 18]. The resulting non-linear equation for a wave propagating in one dimension is

$$\frac{1}{c^2}\frac{\partial^2 u}{\partial t^2} - \frac{\partial^2 u}{\partial x^2} = \frac{\partial}{\partial x}\left(\frac{\beta}{2}\left(\frac{\partial u}{\partial x}\right)^2\right), \tag{2.32}$$

with $x \equiv x_1$ the direction of propagation and $u \equiv u_1(x_1, t)$ the respective displacement, where the index indicates the axis of a Cartesian coordinate system and t time. c_P is the phase velocity of the longitudinal wave and β denotes the non-linearity parameter. Assuming a harmonic wave like in Section (2.1.2.2) with the first order

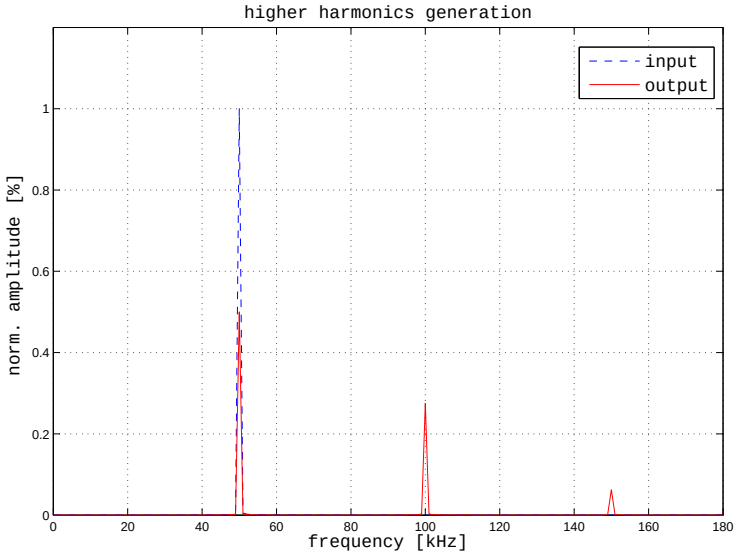

Figure 4: FFT of input and output signals

amplitude A_1 and the corresponding second order amplitude A_2 the right-hand-side of this equation can be developed resulting in the relationship for β,

$$\beta \propto \frac{A_2}{k^2 x A_1^2}. \tag{2.33}$$

The non-linearity parameter holds a direct relationship to the level of damage of the specimen and represents a dimensionless parameter for non-linearity characterization of the investigated material, which makes it very important for this work. By means of the relationship (2.33) it can be seen, which parameters can be varied to detect the non-linearity of the object under investigation. Several techniques will be considered in this work in order to confirm the feasibility of measuring the nonlinearity constant of concrete materials using surface waves.

2.2.1 Nonlinear evaluation methods

Nonlinear acoustics methods deal with the changes of the incident signal that occur, when the wave is propagating through or along the surface region of the material. A considerable amount of comparative studies has been made between linear and

nonlinear techniques and can be found in the literature [2, 4, 25, 28]. The common results state that nonlinear techniques are much more sensitive to material micro-scale damage and distributed damage and therefore are better applicable for detection of early stage damages. Most of the nonlinear nondestructive material evaluation methods for concrete rely on frequency domain analysis of stress waves that have propagated through the material. Payan et al. [25] used nonlinear resonant ultrasound spectroscopy (NRUS) to asses thermal damage in concrete. Accordingly the shift of the resonant peak frequency respond to increasing exciting amplitude was investigated. A significant sensitivity to thermal damage in concrete compared to linear techniques like velocity measurements was demonstrated in that paper. Others investigated the propagation of finite amplitude waves through materials, observing a generation of higher harmonics and parametric mixing due to intrinsic nonlinearity [5, 10, 15, 17, 22, 31, 33]. The main effect is a shift of spectral energy from the frequency of the probe towards different frequency-components. The amount of the energy shifted can also be directly related to the amount and extend of intrinsic microcracks and consequently the scale of damage [8]. Shah et al. [30] reports a successful evaluation of progressively damaged concrete samples applying a nonlinear ultrasonic technique based on higher harmonics generation. This work points out that the third harmonic is much more sensitive to compressive load in concrete than the second. It is furthermore demonstrated that the sensitivity to compressive damage also increases with input signal power level. Warnemuende et al. [33] compared the applicability of passive and active modulation techniques on concrete material showing promising results especially with the latter and Liu et al. [22] showed that collinear wave-mixing method can be used for tracking alkali-silica reaction (ASR) damage in concrete. An alternative technique is introduced by [4], which used the Scaling Subtraction Method to evaluate cylindrical concrete samples that were damaged by compression load. The Scaling Subtraction Method relates a reference signal u_R to the nonlinear material

response of the damaged sample. In this paper it is shown that the technique is very easily applied and reliable in results. Damage could be detected and its evaluation could be monitored. The disadvantage of all these methods so far is that special samples need to be prepared for the measurements. Also most of this authors used through-transmission techniques in their measurements, which makes it mainly applicable to laboratory specimens not to field structures. In this work a field applicable technique shall be developed. For the sake of understanding of performed measurements and analysis the following sections will provide a coarse theoretical overview of the theory behind the used methods and the derivations of the measured nonlinearity parameters.

2.2.2 Nonlinearity parameter for Rayleigh surface waves using second harmonic generation technique

In Section 2.1.2.4 the linear solution of the Rayleigh wave was derived. This chapter will be focused on the nonlinearty parameter for Rayleigh waves, that shall characterize the extend of the material damage. Additionally to previous assumptions the ratio of $\frac{u_s^{(2)}(x_1,x_2,t)}{u_s^{(1)}(x_1,x_2,t)} \ll 1$ from Eq. (2.25) has to hold. For the second order solution several alternatives were derived in literature [12, 16, 19, 23]. For present purposes it is reasonable to follow the derivation of [13]. Therefore, the first order harmonic solutions (2.27) and (2.28) and the second order harmonic solutions for Rayleigh waves, defined as

$$u_1^{(2)}(x_1,0,t) = B_2\sqrt{b_1 b_2}exp\left[i\omega\left(t-\frac{x_1}{c_R}\right)\right], \quad u_2^{(2)}(x_1,0,t) = iB_2 b_1 exp\left[i\omega\left(t-\frac{x_1}{c_R}\right)\right], \tag{2.34}$$

are used. It is known that in an isotropic material acoustic nonlinearity only arises from longitudinal contribution of the wave [13]. Accordingly the in-plane displacement amplitudes of the fundamental and second harmonic of a Rayleigh wave near

surface are related as those in the bulk longitudinal waves:

$$\frac{B_2}{B_1^2} = \frac{\beta k_P^2 x_1}{8}. \tag{2.35}$$

Given that in the experiment only the out-of-plane component of the displacement is measured, the ratio of the second harmonic and the fundamental amplitudes on the surface is

$$\frac{u_2^{(2)}(x_1,0,t)}{\left[u_2^{(1)}(x_1,0,t)\right]^2} = \frac{\beta k_P^2 x_1}{8ib_1\left[1-\frac{2}{(1-b_2^2)}\right]}, \tag{2.36}$$

which can be rewritten into the for this work important relationship for the acoustic nonlinearity parameter for the Rayleigh wave using second harmonic generation technique as evaluation method:

$$\beta = \frac{u_2^{(2)}(x_1,0,t)}{\left[u_2^{(1)}(x_1,0,t)\right]^2}\frac{8ib_1}{\beta k_P^2 x_1}\left[1-\frac{2}{(1-b_2^2)}\right]. \tag{2.37}$$

It shall be noticed that this equation contains a contribution from the interaction between the components of shear and longitudinal waves, although the acoustic nonlinearity for the shear wave itself vanishes due to symmetry of the third order elastic constants.

2.2.3 Principle of signal modulation in nonlinear medium

The theory of modulation distinguishes between amplitude and angular modulation. Angular modulation generally involves both frequency and phase modulation. In terms of simplicity we only will focus on frequency modulation in this discussion. In the wave mixing method for material evaluation developed and applied in this work both of the modulation processes take place at the same time. In the following amplitude and frequency modulation are described in detail.

2.2.3.1 *Amplitude Modulation*

The mathematical representation of an amplitude modulated function can be written as

$$\eta_a(t) = (1 + c_a(t))m_a(t), \tag{2.38}$$

where $c_a(t)$ is the so-called carrier function and $m_a(t)$ is the modulating function. Both functions are sinusoidal with frequencies f_c and f_m, respectively. When M is defined to be the largest amplitude of the modulating signal and A the constant amplitude of the carrying signal, then we can specify the modulation index as follows:

$$q = \frac{M}{A} \tag{2.39}$$

The equations for the respective signals can be written as:

$$c_a(t) = Asin(2\pi f_c t + \phi_c) \quad and \quad m_a(t) = Mcos(2\pi f_m t + \phi_m) \tag{2.40}$$

For phases set to zero, respectively and with an index of $q = \frac{1}{2}$ a part of a possible representation is graphically given in Figure 5. Expended to its particular parts

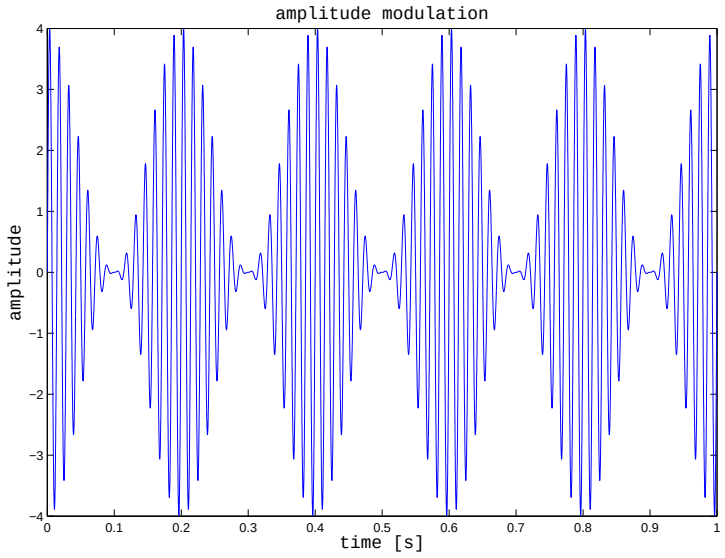

Figure 5: Amplitude modulated signal in time domain

Eq. (2.38) can be brought into a form, where its particular frequency components, generated by the modulation, become obvious. It shall be noticed that now the sum $(f_c + f_m)$ and the difference $(f_c - f_m)$ of the initial frequencies additionally appear in the equation.

$$\eta_a(t) = Asin(2\pi f_c t) + \frac{MA}{2}[sin(2\pi(f_c + f_m)t + \phi_m) + sin(2\pi(f_c - f_m) - \phi_m)] \quad (2.41)$$

In the literature these components, which are slightly above and below the carrier frequency f_c are known under the name "sidebands" and can be seen in the frequency domain plot in Figure 6

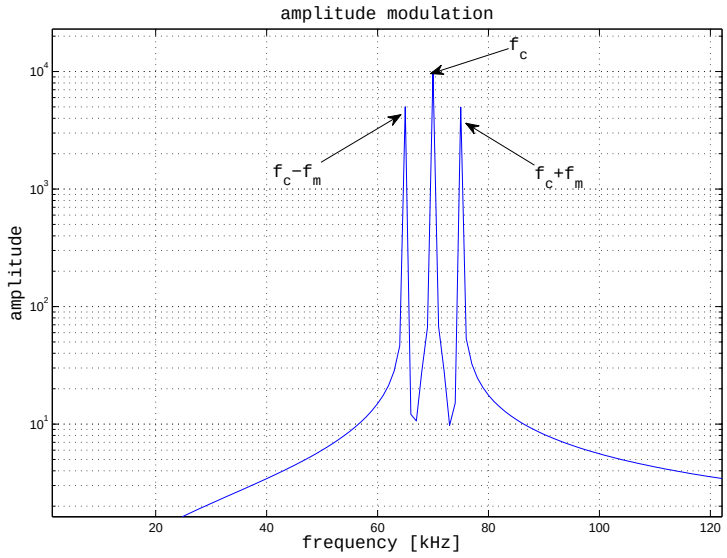

Figure 6: Amplitude modulated signal in frequency domain

2.2.3.2 Frequency Modulation

The frequency modulated signal also requires a carrier signal that can be defined similarly to Eq. (2.40).

$$c_f(t) = Acos(2\pi f_c t + \phi_c) \quad (2.42)$$

A harmonic modulation is assumed here again. The representation of the frequency modulated signal η_f is given by

$$\eta_f(t) = Acos(2\pi f_c t + h_f sin(2\pi f_m t)). \tag{2.43}$$

The factor h_f is the Frequency Modulation Index, specified in Eq. (2.44). Here Δf is the maximum deviation of the instantanious frequency from the frequency of the carrying signal, while f_{max} is the highest frequency present in the modulating component.

$$h_f = \frac{\Delta f}{f_{max}} \tag{2.44}$$

Eq. (2.43) can be expanded to its particular components similarly to those in Eq. (2.41), as well. The main difference in the frequency spectrum however is, that infinite number of sidebands arises around the carrier component. The amplitudes of this sidebands are following the rule of Bessels functions of the first kind [15]. Figure 7 gives an example of a frequency modulated signal in frequency domain.

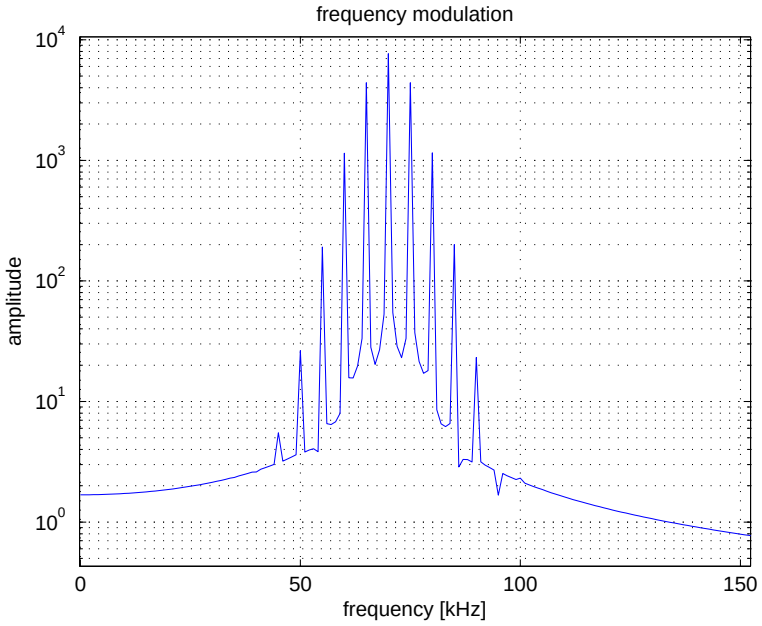

Figure 7: Frequency modulated signal in frequency domain

2.2.4 Active modulation technique

Two major types of modulation techniques can be distinguished in non-destructive material evaluation. The more common occurs when a harmonic wave interacts with passive disturbances like defects of any kind within the material. The biggest adverse effect in applications with concrete is the attenuation, which makes the quantification of the modulated and attenuated energies very difficult, when higher frequencies (> 50 kHz) are used. Also the amount of the modulated energy is generally so small, that high level of damage would be required to see the changes in the spectral analysis [33]. In order to increase the sensitivity to early stage damage active modulation processes are adequate. The higher sensitivity results from controlled and therefore improved modulation of the signal. The particular technique used in this work uses the sum of two sinusoidal functions with different frequencies f_1 and f_2, as written in Eq. (2.45). S_1 and S_2 are the amplitudes, respectively. c is the phase velocity and x the direction of propagation. The nonlinear behaviour of concrete material causes a development of additional frequency components in the power spectrum, Eq. (2.46). The plot in Figure 8 shows a simple example of the process by showing the input-function $\eta_s(t)$, its power spectrum and the power spectrum of the output-function for $(\eta_s(t))^2$. Since only a part of the incident signal energy gets modulated, the resulting spectrum of a material with quadratic behaviour can be pictured as the superposition of both FFTs.

$$\eta_s(t) = S_1 cos(2\pi f_1(t - \frac{x}{c})) + S_2 cos(2\pi f_2(t - \frac{x}{c})) \tag{2.45}$$

The advantage of the active modulation is that now it is predictable which components in the power-spectrum are caused by the nonlinear behaviour of the material. Also advantageous when using concrete material is in fact the generation of the lower frequency component $(f_1 - f_2)$, because the attenuation effect of the heterogeneous material decreases with a smaller frequency. Therefore, the amplitude of the difference frequency component is much easier to measure. The mathematical representation of

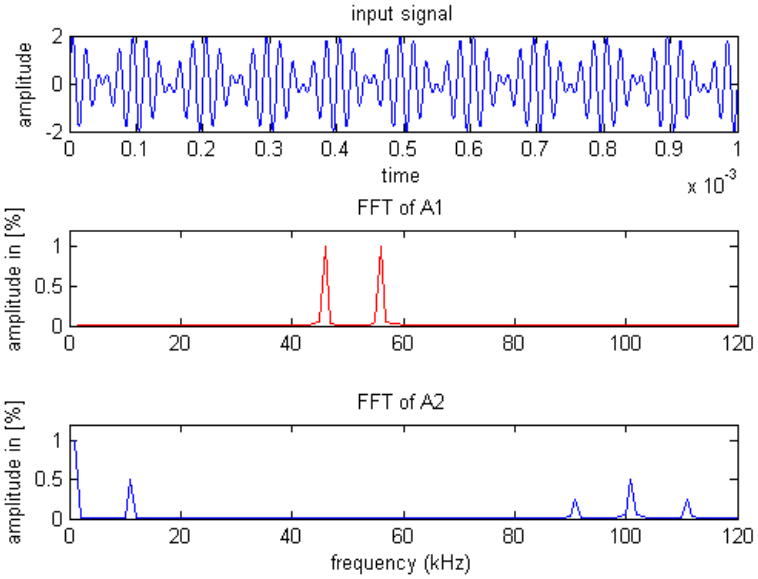

Figure 8: Active modulation

the modulated signal is given below:

$$\begin{aligned}\eta_{s2}(t) = &-\frac{S_1 S_2 \beta \pi^2 f_1 f_2}{c^2} x cos\left[2\pi(f_1 - f_2)(t - \frac{x}{c})\right] \\ &+ \frac{S_1 S_2 \beta \pi^2 f_1 f_2}{c^2} x cos\left[2\pi(f_1 + f_2)(t - \frac{x}{c})\right] \\ &+ \frac{S_1^2 \beta \pi^2 f_1^2}{2c^2} x cos\left[2\pi(2f_1)(t - \frac{x}{c})\right] + \frac{S_2^2 \beta \pi^2 f_2^2}{2c^2} x cos\left[2\pi(2f_2)(t - \frac{x}{c})\right]\end{aligned} \tag{2.46}$$

The component this work will focus on is the first term on the right-hand-side of Eq. (2.46). The respective amplitude will be refered to as S_{mod} in the following.

$$S_{mod} = -\frac{S_1 S_2 \beta \pi^2 f_1 f_2}{c^2} x cos\left[2\pi(f_1 - f_2)(t - \frac{x}{c})\right] \tag{2.47}$$

The non-linear parameter used in the nonlinear wave mixing is defined as

$$\beta \propto \frac{S_{mod}}{k^2 x S_1 S_2}. \tag{2.48}$$

In the real experiment both amplitude and frequency modulation take place, when collinearly mixed waves are introduced to the material. It will be referred to that in the discussion of signal analysis.

CHAPTER III

CONCRETE MATERIALS AND SPECIMEN

This chapter will particularly give a discussion on the examined concrete samples and their properties relevant to the present research.

3.1 Nonlinearity of concrete materials

Concrete in general is a solid material composed of cement, fine and coarse aggregates, sand and water, which makes it a very complex multi-phase material. Due to the strong inhomogeneity and presence of microcracks, which already exist in undamaged state, concrete materials feature remarkable nonlinearity in their elastic behaviour similar to rock and other geomaterials. Microcracks usually occur at the interface of bond between the aggregate and cement mortar already during the curing process. It is obvious that these microcracks are much smaller than the size of aggregate and therefore cannot be effectively detected by standard linear ultrasonic techniques like pulse velocity or resonant frequency. Under applied mechanical, e.g. [4, 30], or chemical, e.g. [6, 7, 28] loads the nonlinearity increases steadily with the growing size and number of microcracks. Finally the degradation can reach an extent that can lead to a fatal failure of the loaded structure. Therefore detection of early stage damage or micro-scale material degradation by nonlinear techniques as discussed in Chapter 2 is very important. In the following the sample preparation and its degradation mechanism are covered.

3.1.1 Mixture and conditioning of the samples

The mixture for the used sample was particularly designed for a time-optimized, accelerated carbonation. The carbonation rate depends on several factors, which need to

Table 2: Mix design

incrediants	ratio
water	350 lb/yd^3
cement	558 lb/yd^3
coarse aggregate	1747 lb/yd^3
fine aggregate	1260 lb/yd^3
air content	2.00%
slump	8 inch
w/(c+s) ratio	0.60

Table 3: Carbonation Parameter

parameter	value
Humidity	60%
CO_2	20%
Temperature	40 degrees Celsius

be considered while manufacturing the specimen. Two specimens of $5.5 \times 8 \times 23.5 in^3$ dimensions from the same mix design shown in Table 2 for experimental purposes and three concrete blocks with a cross area of $5.5 \times 5.5\ in^2$ with a controlled carbonation depth were manufactured. After the mixture was poured in the mould, specimen dried under ambient condition for 24 hours before they first were conditioned in a chamber with 100% humidity and 23 degrees Celsius for another day and then were put into an environmental chamber at 55% humidity and 45 degrees Celsius for another week. The conditioning of the specimens is crucial for putting the specimen into a state, where carbonation can occur with the highest rate possible given the boundary conditions of the equipment and physics. Once the concrete blocks were assumed to be perfectly conditioned, which means to have reached the right solidification and humidity level, they were put into a carbonation chamber, the "Water-Jacketed US Autoflow Automatic CO_2 Incubator" by NUARE. The artificial environment parameters for the accelerated carbonation process are shown in Table 3. The exact choice

of the temperature of 40 degrees Celsius and humidity of 60% is based on former research by [14] and was supposed to guarantee the highest carbonation rate for the by the machine to 20% limited CO_2 maximum concentration. This carbonation chamber was used only for one of the samples, while the second sample remained undamaged.

3.2 Carbonation

Carbonation is considered to be one of the most dangerous damage types for steel reinforced structures and is caused by a chemical reaction of CO_2, water and $Ca(OH)_2$ the naturally high pH of the pore solution drops from typical values around $12.4-13.0$ to a value about 8, which again brings the passive layer covering the steel in an unstable condition and corrosion can take place. The depths of carbonation for the above mentioned three specimen were averaged by using the phenolphthalein technique, as shown in Figure 9. Therefore the specimen were cut and a phenolphthalein solution was applied on the revealed surface. Phenolphthalein has the property to become colorless when the pH of the material drops under 8.2, which means that the coloured areas remain uncarbonated. In this way it could be estimated, how deep the carbonation has penetrated in the actual specimen, the depth reached approximately one inch after 5 weeks in the carbonation chamber. Carbonation does not take place in a single reaction, but in a sequence of chemical reactions within the material. In Eq. (3.1) the reactions for the dissolution process of carbon dioxide is given.

$$\begin{aligned} C0_2 + H_2O &\longrightarrow H_2CO_3 \\ H_2CO_3 + H_2O &\longrightarrow HCO_3^- + H_3O^+ \\ HCO_3^- + H_2O &\longrightarrow CO_3^{2-} + H_3O^+ \end{aligned} \tag{3.1}$$

In Eq. (3.2) the reaction of carbonic acid with calcium hydroxide is described [6].

$$H_2CO_3 + Ca(OH)_2 \longrightarrow CaCO_3 + 2H_2O \tag{3.2}$$

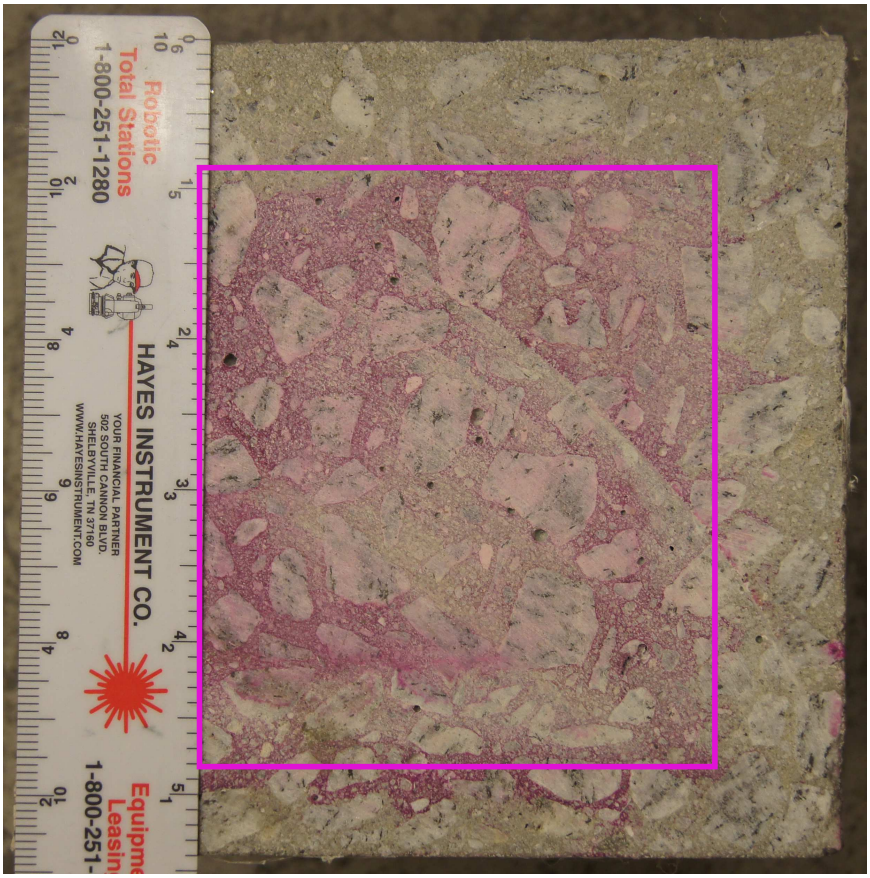

Figure 9: Phenolphthalein test

Reactions (3.1)and (3.2) can only take place in presence of necessary conditions. The rate of diffusion of CO_2 is highly dependent on the water content in the pores. When the pores are fully filled with water, carbonation is mostly missing because of the low diffusion rate of CO_2 and when the pores are dry dissolution of CO_2 cannot take place either. This circumstances make the humidity of the material a decisive factor for the carbonation rate besides the pore structure and temperature [6, 26, 27]. The optimum values are between $50 - 65\%$.

For ultrasonic testing, it is fundamental that these reactions taking place in concrete change the material properties. The reaction of calcium hydroxide with the carbonic acid results in the formation of calcium carbonates. This product features lower density and higher mechanical strength and elastic moduli [6, 11, 24, 26]. This in turn

means that the overall porosity is decreased by carbonation. Furthermore Fabbri et al. [11] have shown that consolidated microcracks generation occurs in the vicinity of the carbonation front, which in turn locally decreases the mechanical properties. It already was mentioned in Chapter 2 that increased nonlinearity is directly related to the amount of microcracks and can be measured through the hysteretic properties of the material using ultrasonic waves.

CHAPTER IV

EXPERIMENTAL SETUP FOR THE SECOND HARMONIC GENERATION METHOD

Two very different concepts were investigated in this work with respect to feasibility of measuring the nonlinearity change of concrete samples due to carbonation. The main criteria for both of them was their applicability to concrete structures in field. One potential method was derived from [13], where Rayleigh surface waves are to assess material damage in nickel-base superalloy. For investigation of near surface degradation of concrete this technique had to be adopted to the conditions in concrete which are very different from those in nickel-base superalloy. In this chapter the experimental setup, procedure and signal processing for the second harmonic generation using Rayleigh surface waves in concrete will be discussed in detail.

4.1 Wedge-Transducer and Rayleigh wave speed determination

In NDT several methods exist to excite an RSW. Some of them include a cascade of transducers or need geometrical specialities of the specimen. The method that will be used in this work is known as the wedge-transducer-method, Figure 10. To be able to apply this relatively undemanding method the exact critical angle has to be known. In the literature it can be found that the RSW speed for concrete materials varies close around $2500 m/s$, which gave the starting point for the design of the wedges. It has also been already discussed in Section 2.1.2.3 that the phase velocity of the longitudinal wave through the wedge material has to be lower then the RSW speed of the specimen. Teflon with a longitudinal wave speed of $1450 m/s$ is the material that meets the requirements for the wedge-material best. By measuring the time of flight

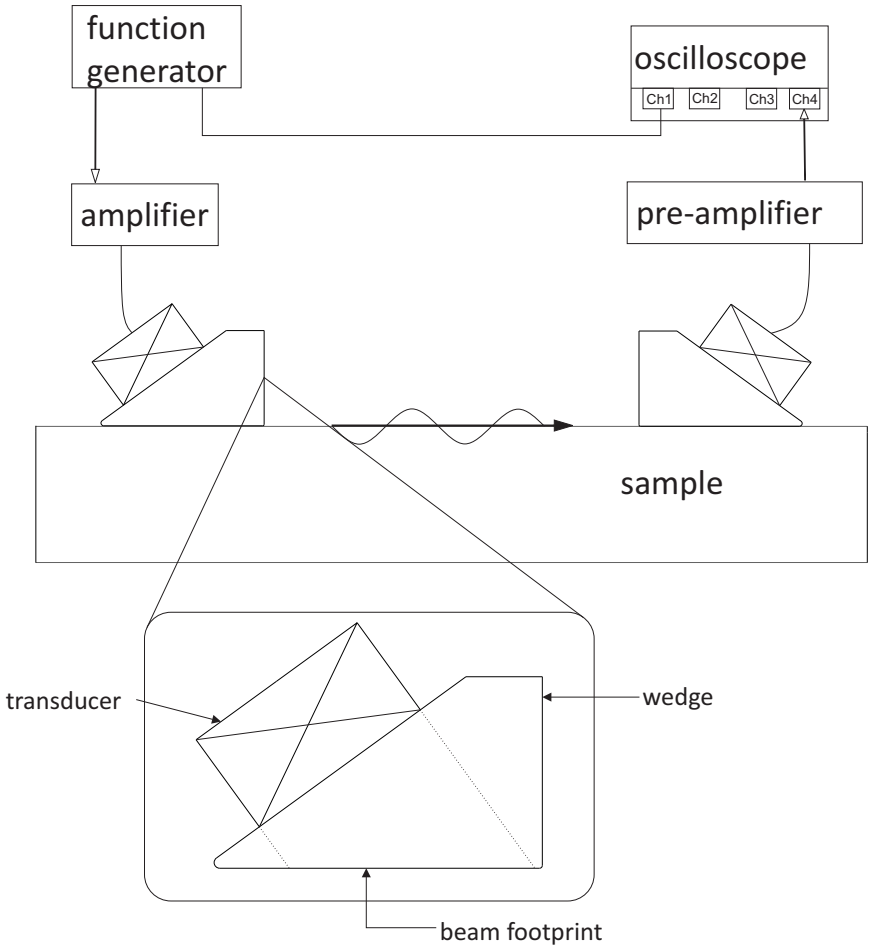

Figure 10: Experimental setup for the second harmonic generation method

of the signal along the surface of the specimen, Figure 11, the wedge angle could be adjusted iteratively. The measured RSW speed for the used specimen was determined by varying the propagation distance and amounts to

$$c_R = \frac{\Delta s}{\Delta t} = \frac{0.05m}{2.04082 * 10^{-5}s} = 2450m/s, \tag{4.1}$$

which results in a critical angle, following Eq. (2.22), of 36.29 degrees.

4.2 Experimental procedure

Rayleigh Surface Waves are excited and detected by wedge-transducers located on the flat surface of the specimen and coupled by *HIGH VACUUM GREASE*, by Dow

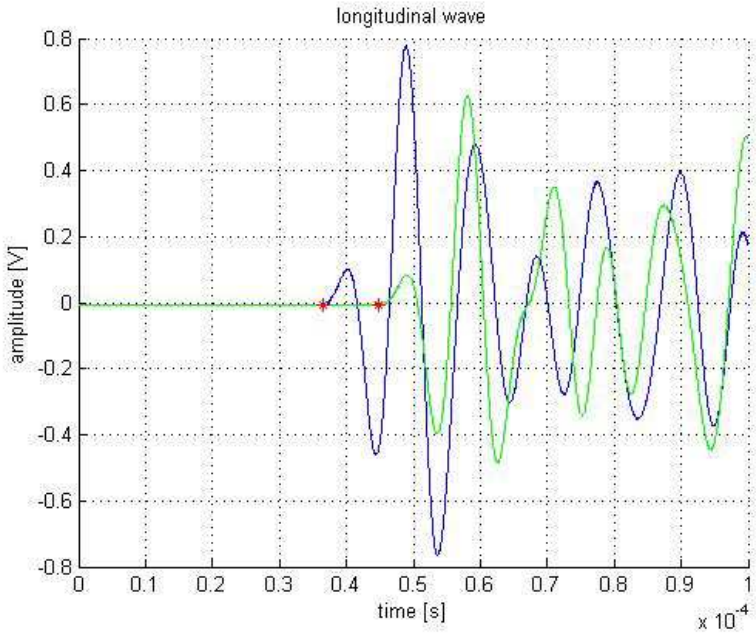

Figure 11: Rayleigh wave speed measurement

Corning, on both transmitting and receiving side. The signal generated by the arbitrary waveform generator *AGILENT 33250A* produces a sinusoidal toneburst of the prescribed frequency, which propagates a certain distance through the material. To increase the amplitude of the incident signal *ENI Model 240LRF Power Amplifier 50dB* is used. The transmitted signals containing the fundamental and higher harmonic parts are detected by a second wedge-transducer. The detected signals are averaged by the *Tektronix TDS5034B Digital Oscilliscope* after the pre-amplification by *Digital Wave amplifier*, and saved for post-signal processing.

4.2.1 Wedge-transducers

For transmitting and detecting the signals, commercial broadband transducers manufactured by Ultran are used:

- Transmitter: Ultran GRD50-D50, 50 kHz, 50 mm
- Receiver: Ultran GRD100-D50, 100 kHz, 50 mm.

The center frequency of the receiving transducer is chosen to be twice the center frequency of the transmitting in order to increase the sensitivity for the second harmonic, which is expected to be smaller than the fundamental by several orders of magnitude. But since a broadband transducer is used, lower frequencies and therefore the fundamental is also reliably detectable. Both transducers have an effective diameter of the active area of 50 mm. Knowing the frequency and the diameter of the source, the far-field distance can be estimated to avoid near-field effects of the evolving wave field. Considering the 50 mm diameter of the transmitting transducer and a signal frequency of 50 kHz the far-field distance yield 102.04 mm, however if the beam of the transducer spreads out in the wedge to a 70 mm diameter, then the far-field distance almost doubles. Since it is unknown what the actual dimensions of the footprint are d_f has to be found experimentally.

$$d_f = \frac{2D^2}{\lambda}, \tag{4.2}$$

where D represents the diameter and $\lambda = c/f$ is the wavelength. d_f is the far-field distance.

4.2.2 Measurement procedure

The transmitting wedge-transducer is positioned and fixed the position on one end of the specimen during one measurement set. Between the surfaces of the wedge and specimen *HIGH VACUUM GREASE* is applied and the wedges are pushed firmly down towards the specimen surface to reduce the acoustic energy losses. In order to measure the material nonlinearity the propagation distance between the two transducers is varied. Since the receiving wedge-transducer is moved in a measurement set to change the propagating distance an equally distributed grease film has to be applied to the complete area where the receiver is wanted to be moved along. The vacuum grease is very viscous and therefore has to be laid on carefully to ensure as uniform film thickness as possible. When distance changed the receiver is pressed down for

several seconds to squeeze out redundant grease between the surfaces. Before taking the measurement the surface where the wave propagates along is cleaned from grease as good as possible to reduce side effects. To ensure, that the wedge-transducers are aligned a ruler is used as an edge guide and measurement tool while changing the propagating distance. The effect of misalignment is discussed in more detail in [32]. When the transmitter and receiver are aligned and the propagation area cleaned 200 measurements are taken and averaged to increase SNR. After the averaged signal for a particular propagation distance is saved the receiver is moved to the next point and the procedure starts all over again. This is repeated for all distances.

4.2.3 Signal generation and signal processing

4.2.3.1 Signal Generation

AGILENT 33250A arbitrary waveform generator is used to produce toneburst signals of 30 cycles. The large number of tonebursts was chosen to increase the accuracy of the measurement and to introduce a sufficient amount of acoustic energy into the propagating wave. Note that this is also one of the fundamental requirements for generation of second harmonic signals. The sufficiently high number of tonebursts also allows extracting the steady state portion, Figure 12 of the signal neglecting the transient part at the very front of the signal and the ringing effect at the end. The strength of the input signal was varied for whole measurement sets in order to achieve a trade-off between large enough amplitude to initiate nonlinear behaviour of the material and loading of the transducer. In the following we will only consider the function generator amplitude of 300 $mVpp$. Before exciting the transmitter the signal is amplified by +50 dB. The actual voltage arriving at the transducer can be read from Figure 13. The detected signal is pre-amplified in a range of $27 - 39$ dB, depending on the signal strength, and recorded by the *Tektronix TDS5034B Digital Oscilliscope* with a length of 25000 points. The recorded signal is saved and processed in MATLAB.

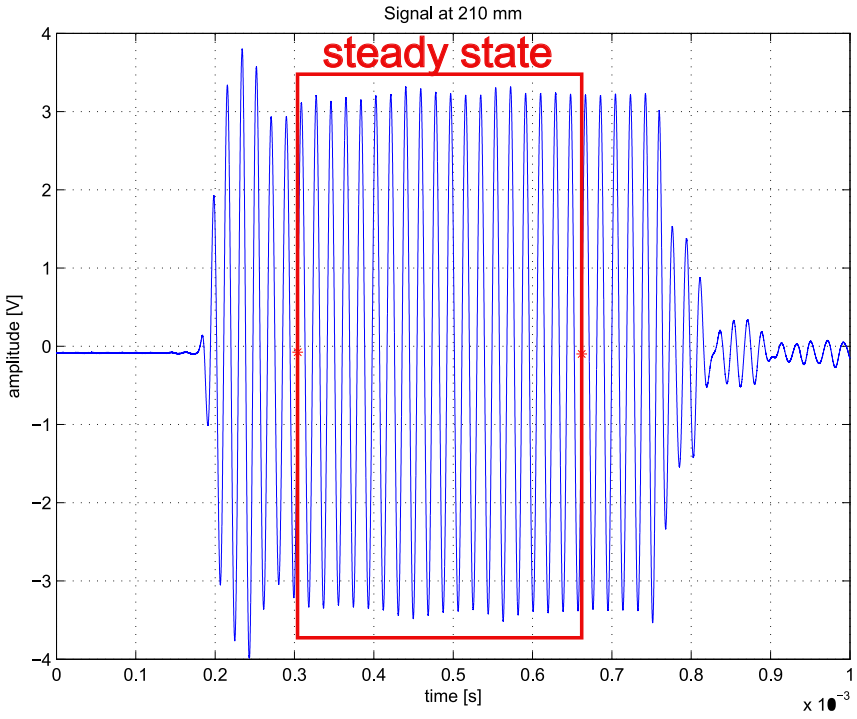

Figure 12: 30 cycles toneburst after 210 mm propagation

4.2.3.2 Signal Processing

To obtain a reasonable Signal to Noise Ratio (SNR), 200 independent measurements are taken and averaged. The averaged signal first undergoes a windowing process using an Hann Window. A 64-point Hann-Window can be seen in Figure 14. The windowing is only applied to the steady-state portion of the signal, the rest is multiplied by zero to obtain a higher resolution in the frequency domain by interpolation. More detail about advantages and the process of windowing in signal processing can be found in [1]. The windowed signal, as shown in Fiq. (15), is subjected to a Fast Fourier Transform (FFT), which gives the frequency domain representation of the received signal, as shown in Figure 16. In this way the amplitudes of the fundamental and second harmonic can be extracted and set into relationship described in Eq. (2.33). By repeating this procedure at different propagation distances, a plot like in Figure 17 can be obtained. The fundamental and second harmonic amplitudes

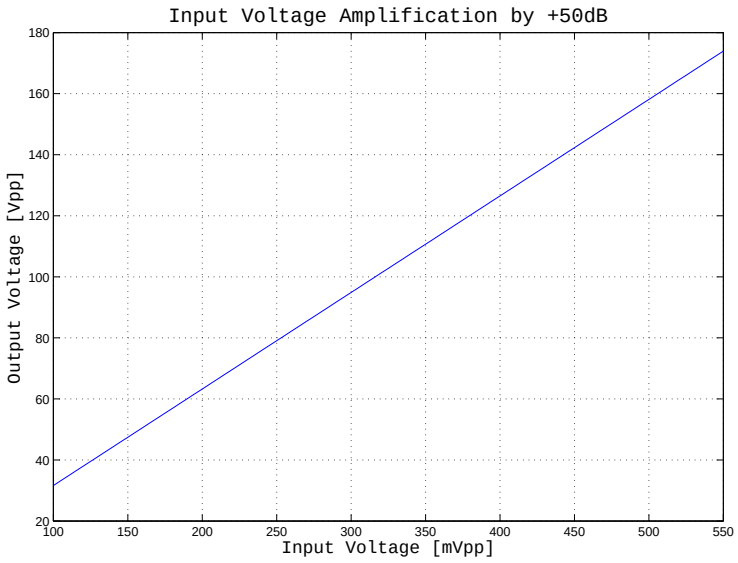

Figure 13: Output voltage after 50 dB amplification

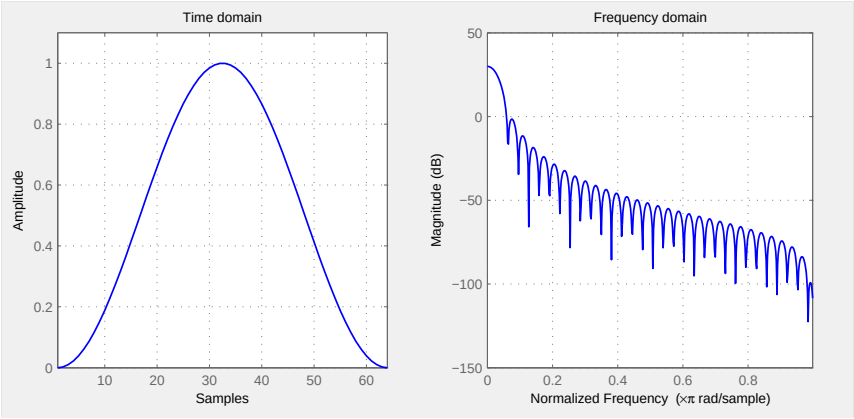

Figure 14: 64-point Hann Window

are labelled as A_1 and A_2, respectively. The relationship (2.33) states that the nonlinearity parameter β is proportional to the normalized second harmonic amplitude A_2/A_1^2. Which means, that the slope of the linear fit in Figure 17 can be interpreted as the expression of nonlinearity of the material, and will be compared in the following results to analyse the nonlinearity of investigated specimen.

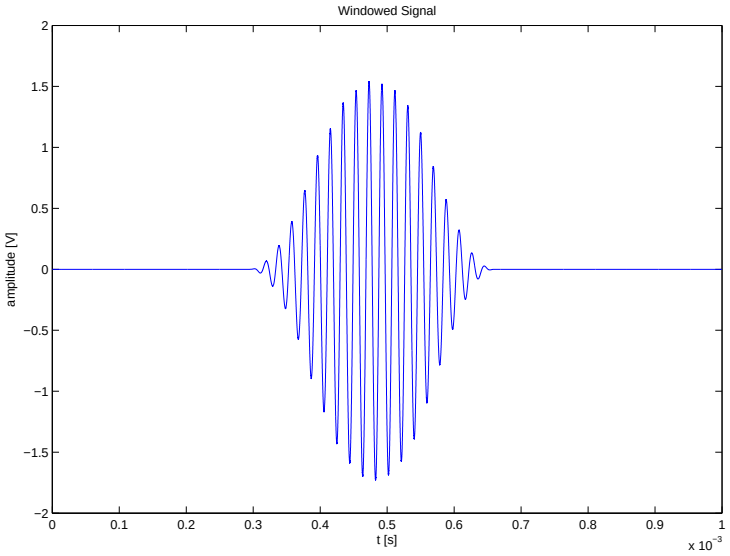

Figure 15: Windowed signal

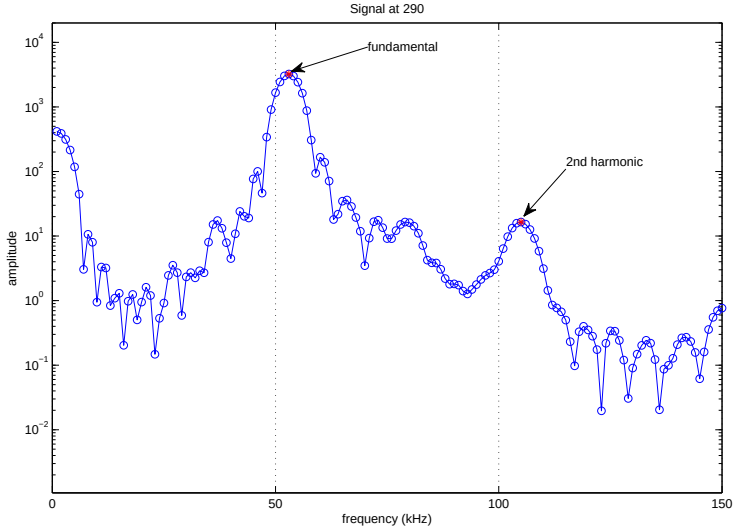

Figure 16: Frequency spectrum of a signal at 290 mm

4.3 Repeatability

Because of the relatively complex experimental setting, complex material properties, possible local effects and also because of the fact that the receiving transducer is to be moved during the measurement procedure, repeatability studies of the experiment

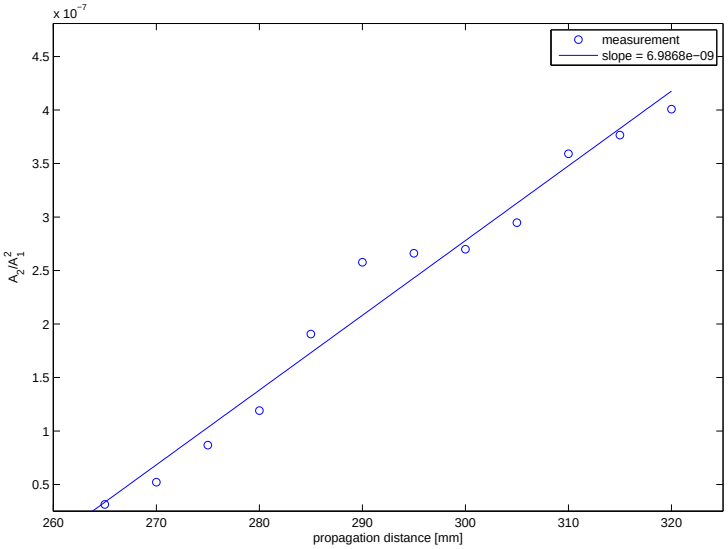

Figure 17: Normalized second harmonic amplitude

had to be done. To ensure that the obtained results are consistent and reproducible at least three measurements were taken along the same propagation line on the concrete sample and the results were compared with each other in respect to behaviour of the fundamental, second harmonic and their ratio, the normalized second harmonic over the propagation distance. Between the measurements the complete setup was removed and repositioned at the same initial locations again.

The second aspect of the repeatability study is the test whether the harmonics, and herewith the nonlinearity parameter, show similar behaviour within the same specimen, but along different propagation lines. Therefore the transmitter and receiver were moved parallelly to the initial propagation line.

CHAPTER V

EXPERIMENTAL SETUP FOR WAVE MIXING METHOD

The general idea behind this method is very different from the one used in Chapter 4. Except for the oscilloscope, that was replaced by *Tektronix TDS 420*, and receiving transducer, that was replaced by the *PCB 353B13* accelerometer or an air-coupled microphone, the same equipment for generation of the signal and data acquisition could be used.

5.1 Transmitter and receiver

For this method several completely different sensors were used to detect the signals, according to Chapter 4 the same transducer with 50 kHz center frequency was used to transmit the signal. For detection of the signal a broadband air-coupled microphone, *G.R.A.S. 40BE* with a broadband up to 100 kHz and an accelerometer, *PCB 353B13*, with a broadband frequency up to 10 kHz and a very flat slope in the stopband are used.

5.2 Measurement procedure

5.2.1 Accelerometer setup

As already explained in Section 4.2, the transmitter is a wedge-transducer positioned at one end of the specimen and is coupled with a vacuum grease to the concrete surface. The accelerometer is coupled by epoxy to the concrete sample and is not being removed during one measurement set. Epoxy coupling provides very high sensitivity for detection of the signal. Since the reception of the wave takes place at a fixed propagation distance of 435mm, the amplitude of the input signal is varied by the function generator in 5 $mVpp$-steps in a range from 100 $mVpp$ to 400 $mVpp$. Before

introducing the signal to the transmitting transducer the signal is subjected to an amplification by +50 dB, as already mentioned in the previous chapter. The actual applied voltages can be read in Figure 13. The signal received by the accelerometer is preamplified by $+19dB$ after propagating along the material surface and is averaged over 300 individual measurements to increase the SNR before being recorded by *Tectronix TDS420 Oscilloscope*.

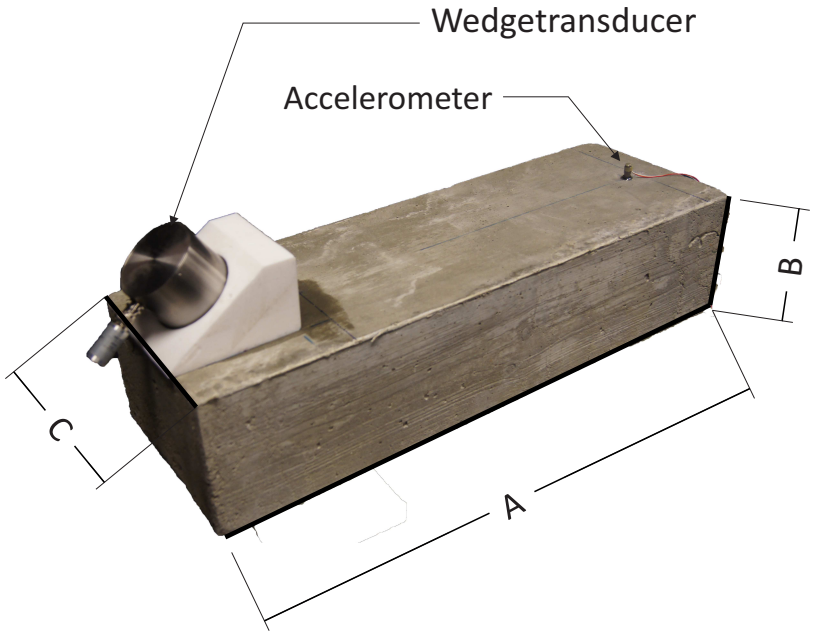

Figure 18: Accelerometer setup

5.2.2 Microphone setup

The second receiver that was tested is an air-coupled microphone. Same transmitting equipment is used. But while the accelerometer is just positioned normally to the surface of the specimen to measure RSWs, the microphone needs to be adjusted in its angle in respect to the surface following Eq. (2.22), similarly to a wedge-transducer, since now there is a second material, air, to be considered in the experimental setup. The angle can be calculated by Eq. (2.22) and results in e.g. 8 degrees. The position

of the microphone is varied over distance along a drawn line to keep the nonlinearity effects of the system as low as possible and keep aligned with the transmitter. The input amplitude is being kept constant at 300 $mVpp$. After propagation preamplification of +39 dB increases the signal strength before recording with the same *Tectronix TDS420 Oscilloscope*. Furthermore the microphone was used for constant distance measurements following the procedure like described for the accelerometer except that the amplitude is varied between $160 - 300$ $mVpp$ and a preamplification of +39 dB is applied. The frequency response of the microphone covers all frequencies of interest. Details will be discussed Chapter 6.

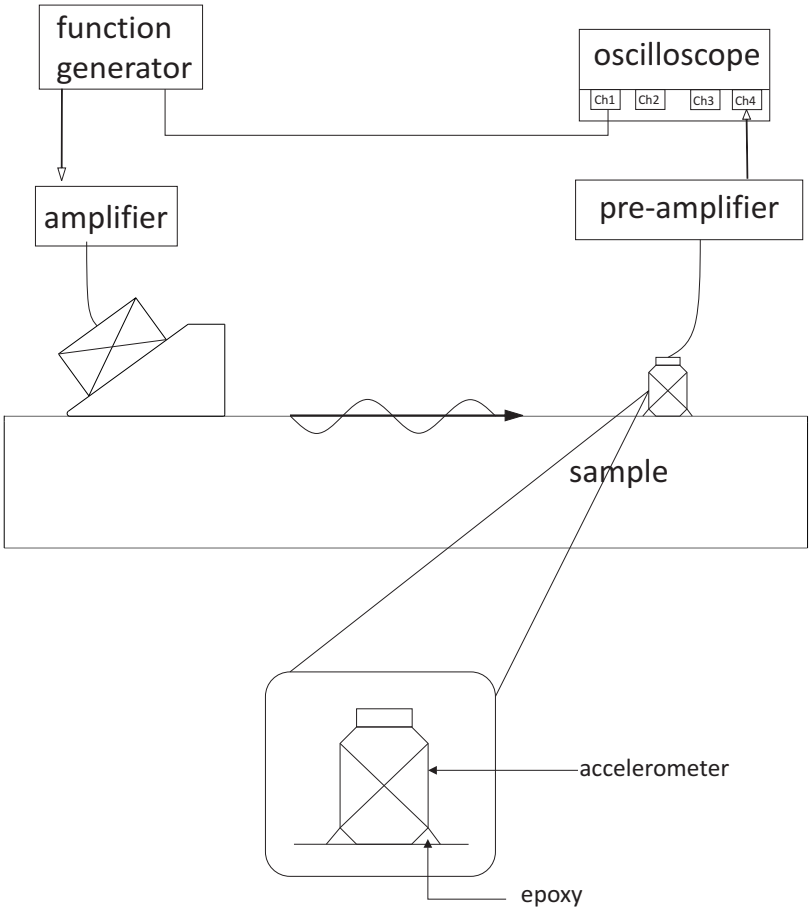

Figure 19: Experimental setup for the wave mixing method using an accelerometer

5.3 Signal generation and signal processing

5.3.1 Signal generation

The speciality of this method is that two individual waves carrying different frequencies are propagating through and interacting with one another in the material. This process is called nonlinear modulation, see Sections (2.2.3) and (2.2.4). The mixing of two or more waves can be achieved in different ways, e.g. using several transmitting transducers, or a combination of a transducer and an impact hammer [10]. In this work the arbitrary waveform generator *Agilent 33250A* is used to generate a mixed wave. Therefore a MATLAB-code had to be written and implemented in the experimental procedure. This code allows importing any possible pair of monochromatic waves with prescribing properties like amplitudes, frequencies and phases to the function generator and herewith expands the number of possible combinations of input signals to infinity. Because of the limited amount of time for this work only a couple of combinations were tested to make the conclusions. The superposition of two chosen waves is downloaded to the function generator, which excites the transducer. The only limitation is, that the center frequency of the transmitting transducer is announced to be $50kHz$, and therefore the fundamental frequencies of the two waves should not be too far away from it. To simulate a toneburst-input zeros were added to the signal after a particular nonzero signal length of 1.5 ms, Figure 20. One downloaded signal has the length of 4.5 ms.

5.3.2 Signal processing for accelerometer setup

The interaction of the propagating waves with material nonlinearities and the resulting wave distortion and modulation occurs as described in Section 2.2.4. The accelerometer received signal could look like plotted in Figure 21, where a particular signal at 250 $mVpp$ can be seen. Unlike in the methods where the signal is not constant in the same position but is moving in the time domain because of changing

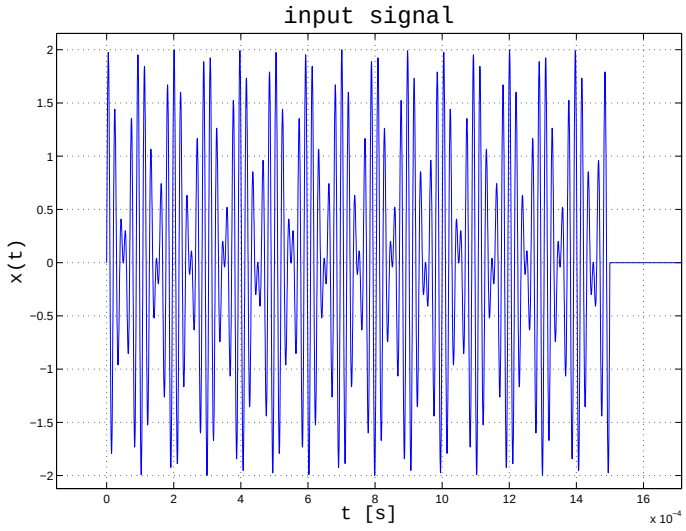

Figure 20: Input signal using a 56 kHz-46 kHz pair

propagation distance, here the interval is fixed for a time window between $5-6$ ms. This procedure is repeated for every input voltage within the range of interest in 5 $mVpp$ steps. The averaged signal is saved and postprocessed using a MATLAB code, see Section 4.2.3.2. The additional frequency components in the spectrum generated by the nonlinear modulation are of interest. The most interesting component for this work is the difference of the two fundamental frequencies, $(f_1 - f_2)$, see section (2.2.4). The difference between the frequencies was chosen after the boundary condition given by the broadband response of the accelerometer of 10 kHz. The red stars in Figure 21 are indicating the interval for post-processing of the signal, which includes the application of the Hann Window and the FFT. Figure 23 represents the obtained result for a signal after windowing and FFT. The amplitudes marked in this plot are taken to build the relation defined in Eq. (2.48). The phase velocity is assumed to be the same for both waves and is therefore neglected. The value defined by this relationship is built for every input voltage and plotted according to Figure 23. Again, the slope of the linear fit of the particular measurements expresses a value that can be related to the nonlinearity of the material. Note that the linear fit is only

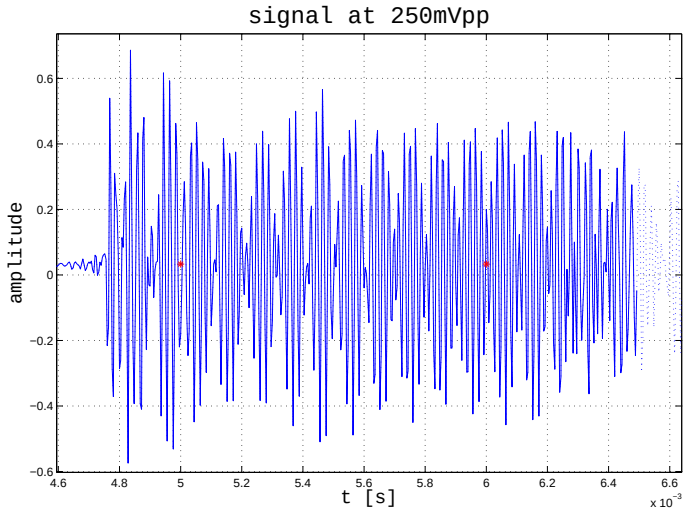

Figure 21: Output signal of the 56 kHz-46 kHz pair at 250 mVpp

made for the range between 160 $mVpp$ and 310 $mVpp$, because after the theory in Section 2.2.4 the relationship between the normalized modulated amplitude of $f_1 - f_2$ and the nonlinearity parameter is supposed to be proportional. The signal processing for microphone setup works as described earlier. The difference for varying distance measurement only is, that the normalized amplitude is not plotted over voltage but over distance. The final plots state similar information concerning the nonlinearity of the material.

5.4 Repeatability

Repeatability test for the setup using the accelerometer was focused on the effects of the epoxy coupling and can be performed very simply. The coupling material gets solidified within 3 min after reaction of both of its components. In order to prove the repeatability of the taken measurements the accelerometer and the transmitting transducer was completely removed, cleaned and reattached again at the same location. After accomplishing this procedure new measurements were taken and obtained

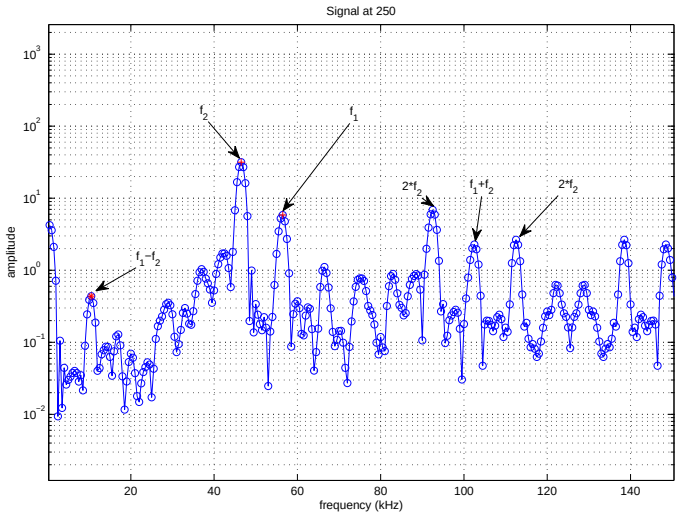

Figure 22: Frequency spectrum of the 56 kHz-46 kHz pair at 250 mVpp

results were compared to former ones. The repeatability of the setup using the microphone is rather complicated. The surface of the specimen is not very even, which makes it hard to keep the distance between the microphone and the surface constant at each measurement point. To ensure the best possible control over that issue, a plastic plate of e.g. $1mm$ thickness was used by slipping it between the microphone and the surface at each point. Hence the setup of the microphone is variable in normal direction from the specimen surface. As explained in Section 4.3, the measurements along one propagation line were taken at least three times under the same conditions to prove the repeatability.

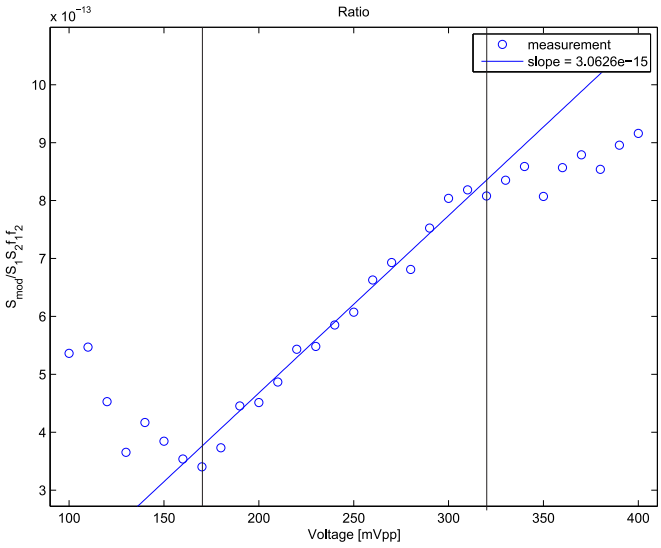

Figure 23: Nonlinearity parameter plot

CHAPTER VI

RESULTS AND DISCUSSION

This chapter is divided into two major sections. In the first, the theoretically expected results and difficulties of the SHG of Rayleigh waves in concrete are discussed. The feasibility results obtained for the normalized second harmonic as well as the repeatability results including the sample evaluation are presented.
In the second section, a discussion on the results of the wave mixing method is provided. Two completely distinct setups for the ultrasonic signal detection are used for this method. However, only the results obtained from the experimental setup using the accelerometer are presented here. A discussion on measurements taken by using the microphone as the receiver is given in the Appendix .0.2.

6.1 Second harmonic generation method results

The method of generating the second harmonic by material nonlinearity in an initially monochromatic signal using Rayleigh waves has been thoroughly investigated in the last few years [13, 32]. Different damage mechanisms are discussed and clear results are presented. However, only metals like A36 steel and nickel-based superalloys, which are highly linear in comparison to concrete and rock materials, were mainly used for those investigations. The technique of nonlinear ultrasonic measurements developed over the years has reduced experimental setup uncertainties like coupling, its viscosity effects, equipment nonlinearities, etc.. The application of the wedge-transducer technique is quite new for concrete material applications and has to be therefore investigated in more detail. In addition, this method has the theoretical advantages of the averaging effect for the signal over a finite area, that is covered by the elliptical transducer beam footprint. Using the wedges, a larger amount of

acoustic energy can be transmitted to excite the actual Rayleigh wave along the surface. In the following, the first feasibility results of this technique as applied to concrete specimens are presented.

6.1.1 Dependence of nonlinearity on propagation distance

For the feasibility tests of the second harmonic generation in concrete, the measurements are taken from a different concrete block than the one discussed above. Its dimensions are slightly larger than those of the actual specimen, $10in \times 10in \times 24in$. The mixture is unknown in detail, but is highly similar to the one discussed in Chapter 3, with the exception of the w/c-ratio.

In this work, the measurements of material nonlinearity using SHG method are performed by varying the propagation distance. The transducers used are naturally nonlinear, and apparently therefore the second harmonic component is already excited by the transmitter. The equipment used generates nonlinearity as well. However, since the input voltage is constant and only the propagation distance of the Rayleigh surface wave is changed, the nonlinearity of the involved instruments remains constant, while the material component of the measured nonlinearity grows linearly with increasing propagation distance. This is referred to as cumulative nonlinearity. The first step to be taken for these measurements is to find out whether and in what range the normalized second harmonic amplitude exhibits linear growth with the propagation distance. Phenomena such as near-field effects or a dominating attenuation influence the linearity and thus have to be excluded from the analysis. The corresponding plot by Walker et al. [32] can be seen in Figure 24 as a reference and presentation of expected results.

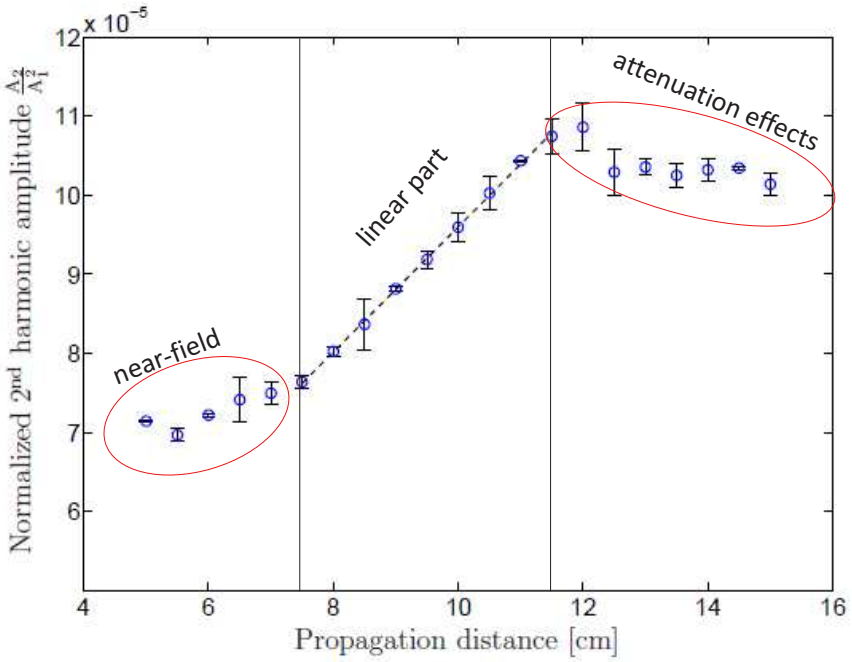

Figure 24: Normalized second harmonic amplitude versus propagation distance for the undamaged fatigue specimen 1. by Walker [32]

6.1.2 Behavior of the amplitudes of harmonics

For simplicity, it shall be assumed that the signal introduced to the material is monochromatic. While propagating through the specimen the immense nonlinearity of concrete causes a distortion of the wave due to interaction with the intrinsic microcracks of the material. While the fundamental amplitude decreases steadily due to attenuation, the higher harmonic amplitudes are expected to grow with the increasing propagation distance, since for longer propagation distance the nonlinearity increases as well. However, the attenuation of the propagating wave in concrete is extremely high, and is dependant on the wave frequency. With a higher frequency and therefore shorter a wavelength, the attenuation grows as well and herewith strongly affects the obtained amplitudes of the harmonics. In other words, the second harmonic is affected much more strongly by attenuation than the fundamental is since

it is at a higher frequency. The domination of attenuation effects of the second harmonic can be observed in numerous measurements, particularly over longer distances. However, it is noted that to obtain a positive slope of the linear part of the normalized second harmonic $\frac{A_2}{A_1^2}$ over distance as in Figure 24, the second harmonic solely needs to decrease more slowly than the fundamental. To obtain a characterization of the material nonlinearity by the second harmonic generation method the fundamental and second harmonic component of the received signal have to be measured. In

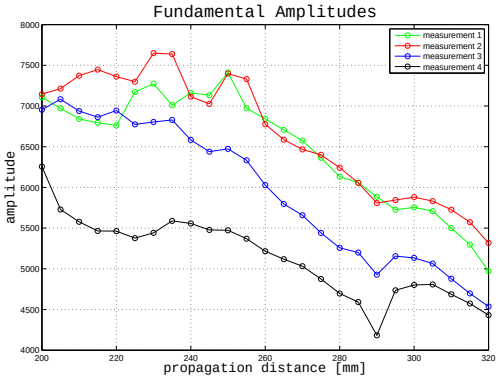

Figure 25: Amplitude of the fundamental over distance

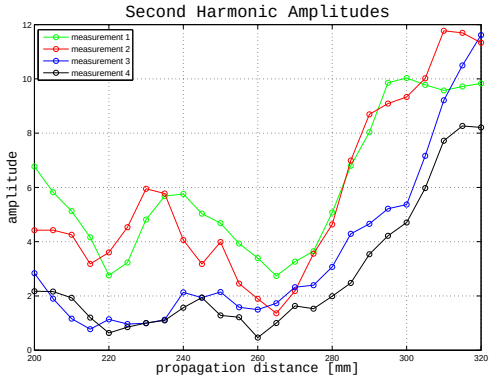

Figure 26: Amplitude of the second harmonic over distance

Figure 25 and Figure 26 the behavior of the first and second harmonic for distance intervals from 200mm to 320mm can be seen, respectively. Up to the distance of 260 mm, near-field effects can be seen in these plots very well. But in the range from 260 mm to 320 mm, the amplitudes follow the expected behavior. The input voltage amplitude for this experiment is 2 Vpp tenfold amplified by *Krohn-HITE model 750 amplifier*. The differences between the measurement sets' origins is in the very different coupling conditions and are usually expected. Nevertheless, the rage of variation is very small, which shows good repeatability of the experimental setup, as seen in Figure 28. It also can be noticed that the fundamental and second harmonic amplitudes are strongly correlated, which leads to the fact that for the actual analysis the second harmonic amplitude is normalized by the square of the fundamental. The

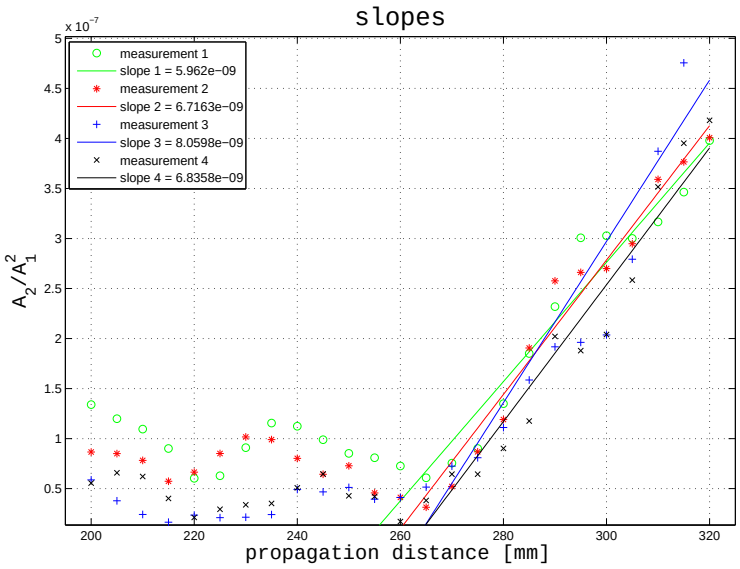

Figure 27: Normalized second harmonic amplitude versus propagation distance for the undamaged concrete sample

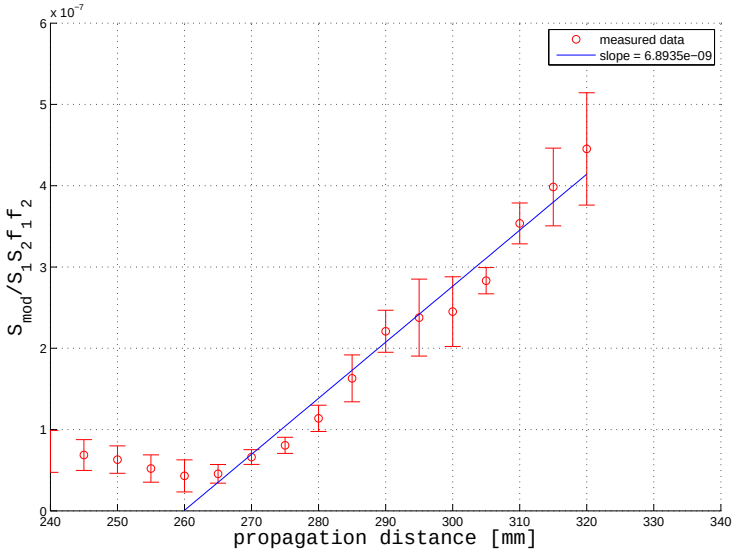

Figure 28: Normalized second harmonic amplitude versus propagation distance for the undamaged concrete sample, averaged

nonlinearity characterization of the material takes place by plotting the normalized second harmonic amplitude over the propagation distance. The obtained relationship

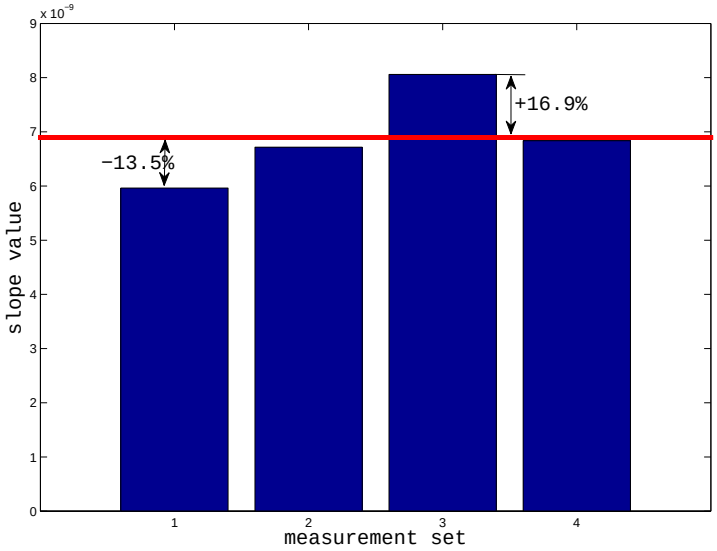

Figure 29: Measured slopes

shows a proportional part after 260 mm, as shown in Figure 27. The slope of this part is directly related to the nonlinearity parameter and is therefore the goal of each measurement set. Figure 29 shows an overview for the measured slopes represented as bars and the red line is their mean value. The maximum value is 16.92% larger than the mean and the minimum is around 13.5% smaller. It is known that for concrete, the nonlinearity measurements can vary within ±20% [20] and therefore the obtained results are within acceptable tolerances.

Due to problems with the equipment used and the low repeatability of measurements taken on different locations of the specimen, this method was not investigated any further.

6.2 Wave mixing method results

One of the most widely used vibro-acoustic methods is combining a high frequency ultrasonic wave with a low frequency vibration mode, [10, 17]. This method counts as a global technique, since the complete specimen is under investigation. Kazakov

et. al [17] combined an ultrasonic probe with an impact hammer to locate cracks and flaws in steel samples, while Warnemuende et. al [33] used a very similar method to monitor microcrack density in concrete caused by a compressive load. This method represents a hardware solution of mixing waves, since two excitation mechanisms are used. In the literature, one also can find software solutions, where only one transducer is used to excite both waves. Liu et. al [22] used this method by taking transmission measurements to detect alkali-silica reaction damage in concrete. Hu et. al [15] used an arbitrary waveform generator to excite two sinusoidal waves simultaneously for detection of cracks in aluminium plates. The mechanism of modulation is already discussed in Section (2.2.3). The propagating wave pair interacts with the intrinsic microcracks, which causes a disturbance in the form that not only the higher harmonics of each wave are generated, but also the so-called side-bands, which represent the sum and difference of the fundamental frequencies.

In the following the results of the setup using the accelerometer will be discussed.

6.2.1 Results of the accelerometer setup

The accelerometer is permanently fixed to one location on the specimen, see Chapter 5, which is aligned to be in the middle of the ultrasonic beam of the transducer. The amplitude of the input voltage is varied by the arbitrary waveform generator from 100 $mVpp$ to 400 $mVpp$, which gives an effective excitation of the transducer in the range between 31.6 Vpp and 126.5 Vpp.

The following procedure is used to develop a field applicable and obtain meaningful results:

1)- prove that frequency components, especially the difference component, can be generated depending on the particular frequency pair

2)- build the normalized difference component for every frequency pair to show that there is a proportional relationship between the input voltage and the

normalized difference component independently from the frequency pair

3)- choose one frequency pair to evaluate both carbonated and undamaged sample

4)- test repeatability of the results

4)- and compare the nonlinearity parameters of undamaged and carbonated samples.

For the first step, a set of frequency pairs, which can be seen in Table (4), is tested in order to show the feasibility of detection of an arbitrary difference component. The pairs are chosen in the way that the fundamental frequencies are not too far away from the center frequency of the transducer and their difference is within the broadband of the accelerometer. Because of the similarity of the results for tested pairs, only four chosen ones will be discussed in this work. For the sake of demonstration, each of the four pairs has a different difference component in the range from 8 kHz to 11 kHz. The second step is aimed at the detection of the fundamental and difference components in the frequency spectrum of each averaged and saved signal for each voltage. From the frequency spectrum obtained, components are set in the relationship for the normalized difference component and are plotted over the input voltage. The first two steps of the development of the technique are visualized in Figures 30-37. It is easily observed that the difference component always arises in the expected location and is simply distinguished from other sidebands or signal processing artefacts. Furthermore the plots demonstrate that the sensitivity of the accelerometer setup is very high. Even though the broadband frequency of the accelerometer is 10 kHz according to its data sheet, second harmonics and the sum of fundamental frequency could be detected with clearly defined amplitudes. It is noticed that in this method the proportionality between the two mentioned parameters is present only for a certain range of voltage amplitudes. Also conspicuous is that the lower limit of voltage is around 150 $mVpp$, which are 47.4 Vpp excitation amplitude. The irregular behavior

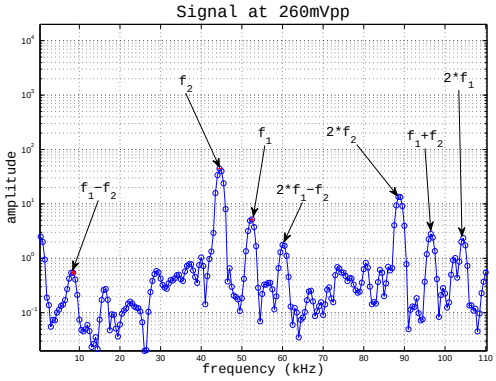

Figure 30: Frequency spectrum of the 52 kHz-44 kHz pair

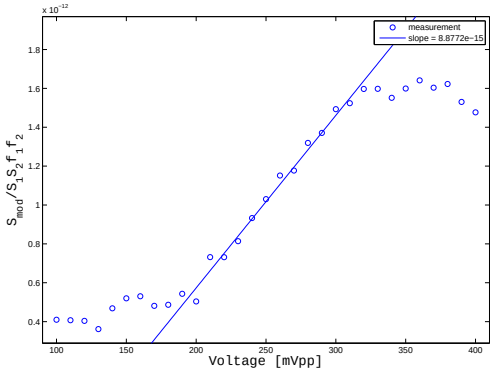

Figure 31: Normalized difference component over voltage for the 52 kHz-44 kHz pair

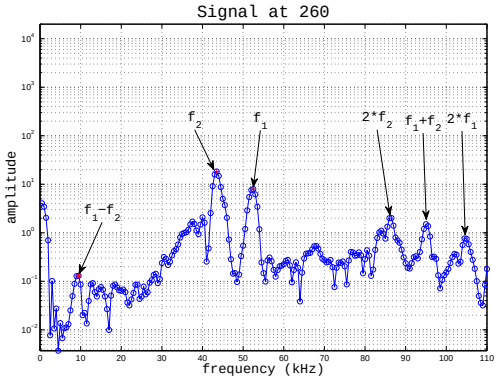

Figure 32: Frequency spectrum of the 52 kHz-43 kHz pair

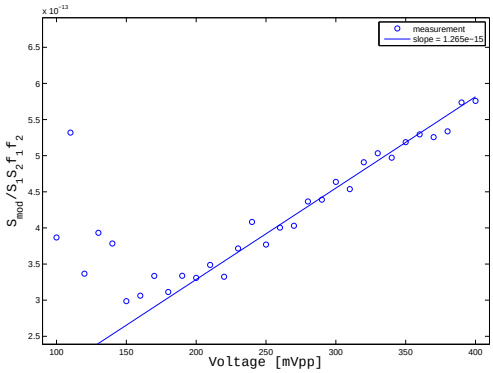

Figure 33: Normalized difference component over voltage for the 52 kHz-44 kHz pair

of the ratio between the normalized amplitude and input voltage for lower amplitudes is already explained in the previous chapters. The nonlinearity in concrete is generated mostly by cyclic opening and closing of microcracks. To induce this effect the amplitude has to be large enough. The upper end of the plot shows irregularities as well. Here a number of different effects are working simultaneously and cannot be clearly separated from each other. On the one hand, there are instruments constraints like a maximum output amplitude of the transducer. On the other hand, the measurement range of the oscilloscope is also limited. The combined effects cause the signal to behave anomalously, as seen in the Figure 38, where the dependency

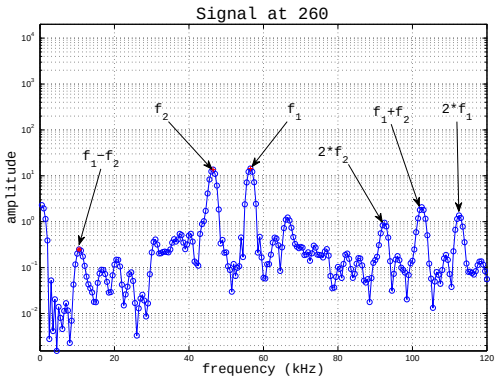

Figure 34: Frequency spectrum of the 56 kHz-46 kHz pair

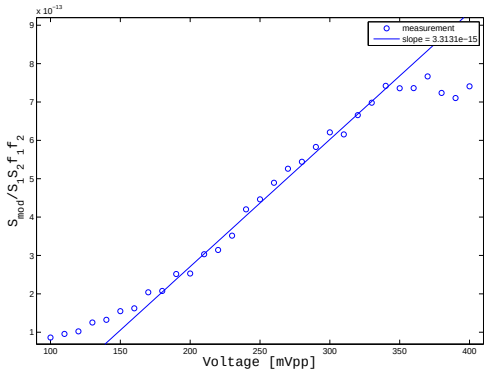

Figure 35: Normalized difference component over voltage for the 56 kHz-46 kHz pair

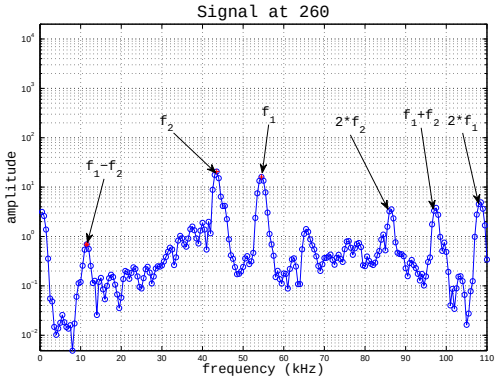

Figure 36: Frequency spectrum of the 54 kHz-43 kHz pair

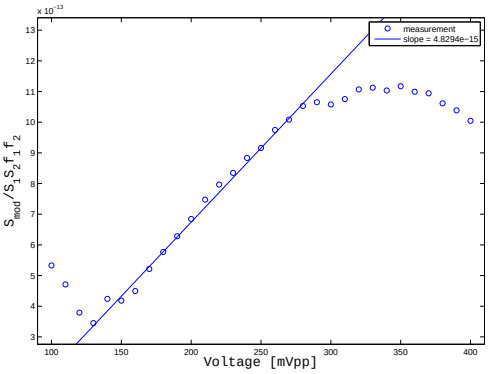

Figure 37: Normalized difference component over voltage for the 54 kHz-43 kHz pair

of the difference component on input voltage is demonstrated for the 52 $kHz - 44$ kHz frequency pair in detail. First, it seems like the difference component is growing quadratically with the increasing input voltage until 300 $mVpp$ (red line), which satisfies the expectations in respect to the nonlinearity parameter. The part encircled by the green ellipse represents the erroneous part. The behavior of the difference component over increasing voltage is compared for all investigated frequency pairs on the uncarbonated sample. Because of the very limited time given for this work, only one frequency pair could be investigated in more detail. The choice of the frequency pair of 56 $kHz - 46$ kHz due to the most consistent results accomplishes the third

Table 4: Frequency pairs in [kHz]

$Frequency f_1$	50	51	51	52	52	52	53	54	54	54	55	55	56	56
$Frequency f_2$	40	53	45	42	43	44	43	42	43	45	44	46	45	46
$Difference$	10	8	6	10	9	8	10	12	11	9	11	9	11	10

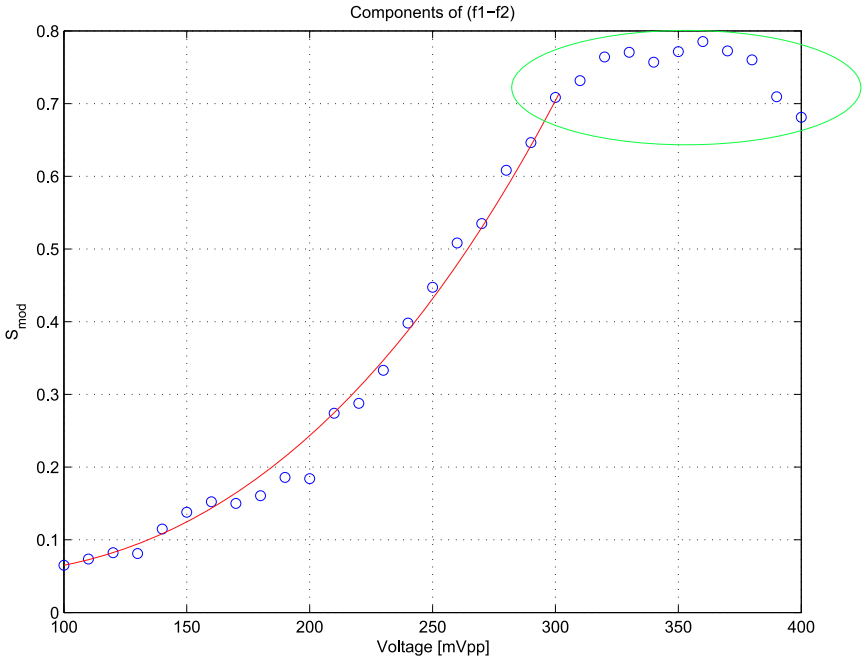

Figure 38: Difference component over input voltage, 52 kHz-44 kHz frequency pair

point in the process. As can be seen in the Figures (39)-(42), the behavior of the product of the fundamental amplitudes grows very linearly for both carbonated and undamaged samples. As well as the trend of the difference component in both cases can be interpreted as quadratic.

6.3 Results of carbonation evaluation

Two specimens are cast from one mixture and are subjected to the same conditioning and drying processes, but one is partly carbonated and the other is not carbonated at all. They are both evaluated using the wave mixing technique determining the nonlinearity parameter. The results from the detection of the difference component

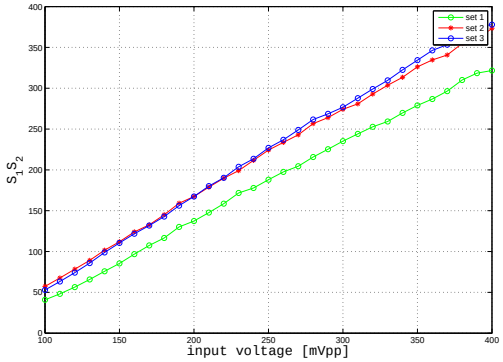

Figure 39: Product of fundamental amplitudes over input voltage, 56 kHz-46 kHz frequency pair, undamaged

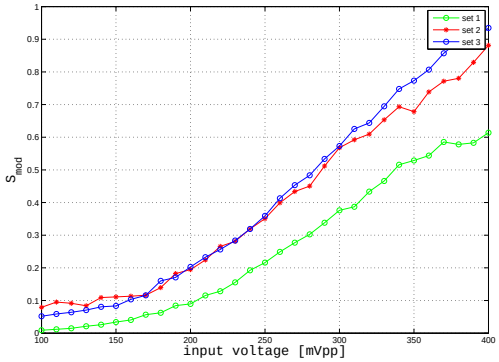

Figure 40: Difference component over input voltage, 56 kHz-46 kHz frequency pair, undamaged

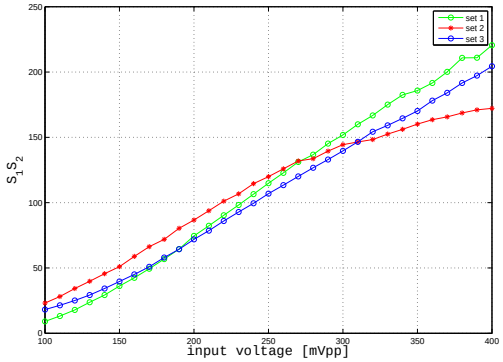

Figure 41: Product of fundamental amplitudes over input voltage, 56 kHz-46 kHz frequency pair, carbonated

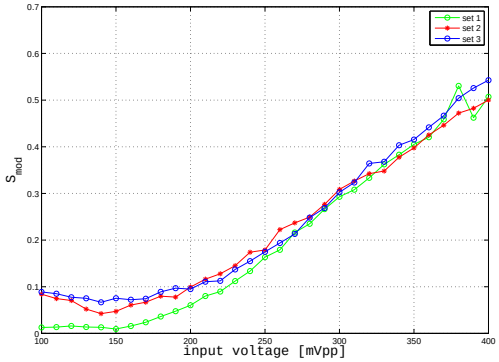

Figure 42: Difference component over input voltage, 56 kHz-46 kHz frequency pair, carbonated

of the fundamental frequencies in the frequency spectrum are already presented in the previous section. The goal of this method is to be able to evaluate the nonlinearity of concrete materials, and in this particular case the nonlinearity change is generated by carbonation. Therefore the last step in the development of the new nondestructive evaluation method using nonlinear Rayleigh waves is to build the relationship between the detected fundamental and difference components for every input voltage, and to obtain the slopes of this relationship, which is directly related to the nonlinearity parameter. The respective plots for the resulting slopes for undamaged and carbonated samples are given in Figure 43 and Figure 44. Three different measurement sets

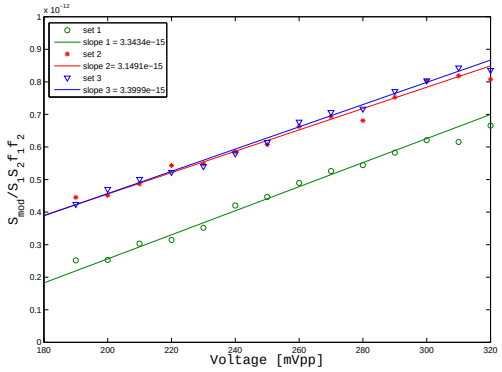

Figure 43: Normalized difference component for single measurement sets over voltage, undamaged

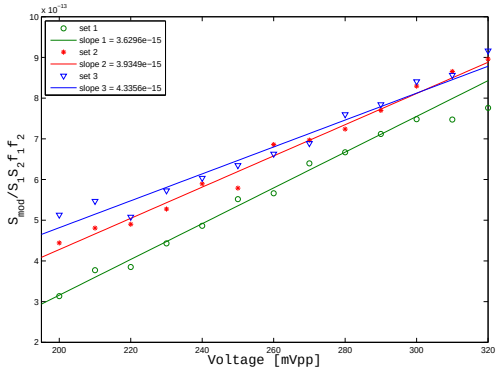

Figure 44: Normalized difference component for single measurement sets over voltage, carbonated

are taken from the carbonated and undamaged sample, respectively, are shown. The offset of the measurement set 1 of the undamaged sample originates from different coupling conditions, however the slope value is very similar. For an overview the slopes are presented in a bar-diagram, like shown in Figure 45. The red errorbars indicate the standard deviation from the mean values. From the slopes it can be

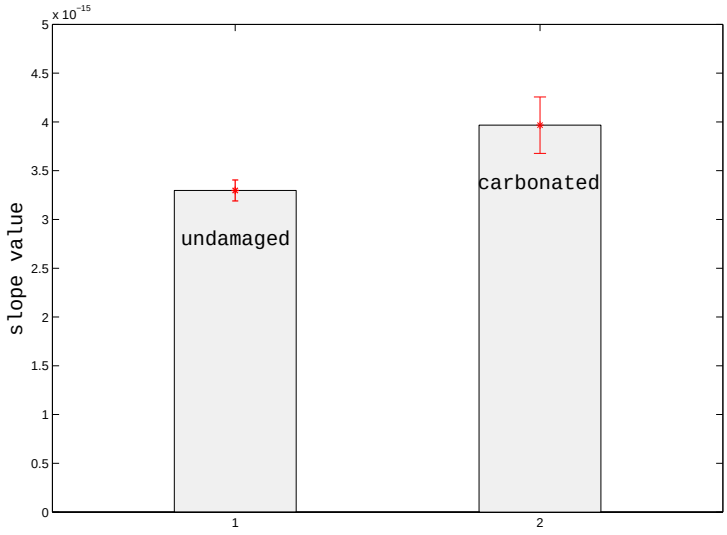

Figure 45: Averaged slope values of undamaged and carbonated samples

seen, that the average slope, and therefore also the nonlinearity parameter is about

Table 5: Measured Slopes

	slope 1	*slope* 2	*slope* 3	*average slope*
undamaged sample	3.3434e-15	3.1491e-15	3.3999e-15	3.30E-15
carbonated sample	3.6296e-15	3.9349e-15	4.3356e-15	3.97E-15

20% higher for the carbonated sample. Furthermore, the plots are presented with the errorbars representation as seen in Figure 46. Here the average ratio between

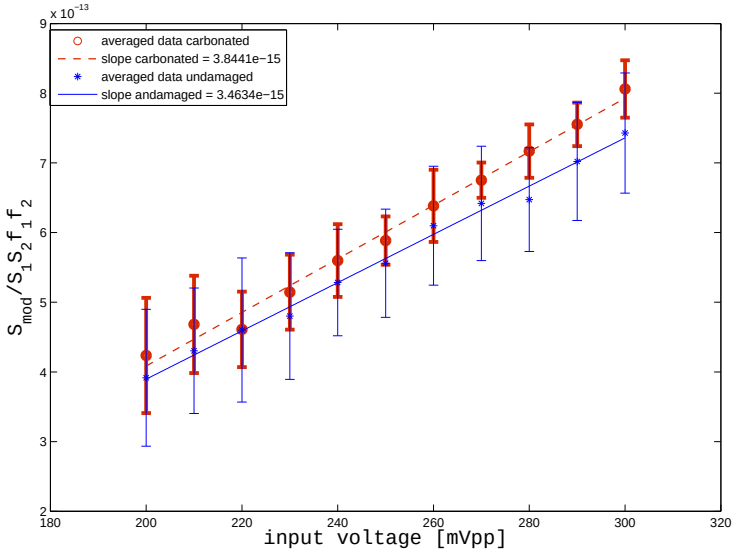

Figure 46: Averaged normalized difference component over voltage, undamaged and carbonated samples

the three measurements for the respective input voltage is built first and the linear fit is calculated by these mean values. The errorbars show the standard deviation. From the calculated slopes, it can be noted that the nonlinearity parameter for the carbonated sample is still about 11% higher. The large errorbars of the undamaged sample in Figure 46 originate from the vertical shift of measurement set 1, when compared to the other two and the relatively small number of taken measurements in that particular configuration.

6.3.1 Repeatability results

As can be inferred from the plots the results of a particular measurement are reproduced very well. The most critical factor for the repeatability testing is the coupling between the accelerometer and sample. The coupling material solidifies within 3 *min* after reaction of both of its components. This has the advantage of consistent coupling behavior, but it also is very hard to remove the accelerometer again. Therefore this coupling method is suitable for permanent attachment to the specimen or the object under investigation. When making nonlinearity measurements of a concrete object in the field, it would be reasonable to always measure the same area to monitor the development of a degradation mechanism like carbonation. In that case epoxy coupling shows certain advantages. For research purposes, especially to investigate the repeatability of the method, it is rather laborious to use this coupling, since the accelerometer has to be completely removed and reattached again, which can damage the surface of the specimen.

CHAPTER VII

CONCLUSION AND FUTURE WORK

Rayleigh surface waves are used in this research to develop a field applicable technique for ultrasonic evaluation of near surface damage in concrete. Two different methods are investigated with respect to feasibility and quality of results. The second harmonic generation method is found to be generally promising, since the fundamental and the second harmonic amplitudes could be detected simultaneously. It also shows advantages like the averaging effect over a finite area for the transmitting signal as well as its detection. However due to instrumental limitations, the investigation could not be continued in the time frame given for this research. The fundamental frequency used in this work is found to be too high and should be reduced for future investigations of this method. Concrete is a highly attenuative material. Attenuation is dependent on the frequency of the signal and therefore the second harmonic is much more affected. By reducing the fundamental frequency, not only the attenuation effect could be decreased, but also local effects, which happen due to the inhomogeneity of the material can be weakened because the wavelength of the signal is larger at with lower frequency. Another aspect in this method is the problem concerning the coupling conditions between the teflon wedges and the specimen surface. More detailed investigations have to be done concerning the affect of the grease layer thickness and pressure level and time applied on the wedge on the detection accuracy. To increase the potential of this promising method to be applied to concrete materials, more work has to be done.

The wave mixing technique for Rayleigh waves propagating along the surface shows a great potential for the evaluation of carbonation damage in concrete. The sum of two

independent sinusoidal waves, driven by two different frequencies, is used to excite a low frequency wave. This wave arises through the interaction of the two ultrasonic waves with the nonlinear material, at the difference frequency of the fundamental frequencies. In this way a very low frequency wave could be generated by still using a $50kHz$ transducer. As a detecting sensor, an accelerometer is used, providing high sensitivity. The difference component in the power spectrum can be detected in all the measurements performed. A comparison between the carbonated and the reference undamaged sample is performed with the result that the nonlinearity of the carbonated sample is larger, than that of the undamaged sample. However, in this work only two specimen are considered. Concrete is a multi-phase material, and its nonlinearity can have significant variability, even before the damage occurs. Nonetheless, the goal was to develop a method that is capable of reliably measuring the nonlinearity of concrete materials using Rayleigh surface waves to make it also applicable in field. The wave mixing technique shows all necessary features to meet these requirements. The nonlinearity of the samples can be reliably measured and the results can be reproduced with a good repeatability. For future work on this method it is recommended to test different coupling materials for the accelerometer, to make the measurement procedure less laborious. The material evalution, e.g. detection of carbonation, has to be performed on more than two samples, also the nonlinearity of the specimen should be measured before and after undergoing the carbonation process, to be able to determine the effect of carbonation on the nonlinearity of the material. The affect of the chosen frequency pair has to be investigated further.

.0.2 Results of the microphone setup

The measurements taken along the propagation path with the microphone have a big advantage of its being non-contact to the surface, which eliminates the cumbersome coupling problems discussed above. However it has to be noted that the surface of any concrete structure is never perfectly even and can have roughness in finite dimensions within even a small area. This surface roughness causes the trouble that the layer of air, which is used as coupling material varies in its thickness as well. The wave propagating through the air quickly loses a lot of its energy and therefore the thickness of the air layer should be constant for consistent measurements.

In the following Figures 47 and 48 the amplitudes of the product of the fundamentals and of the difference component are depicted. Building the relationship for the

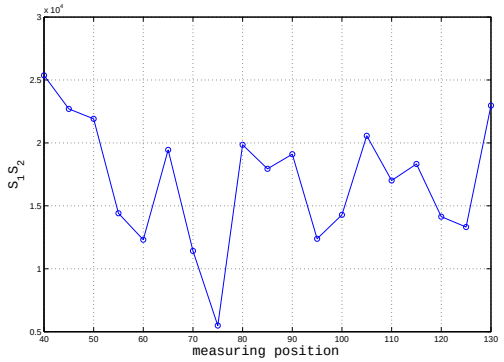

Figure 47: Product of fundamental amplitudes over distance, microphone detection

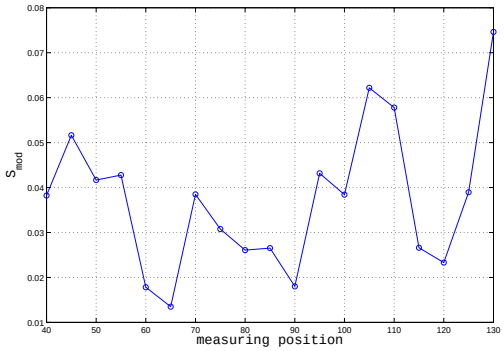

Figure 48: Amplitude of the difference component over distance, microphone detection

nonlinearity parameter defined in Eq. (2.48) and neglecting the differences in the phase velocity of the two wave the plot Figure 50 is obtained. No recognizable dependencies between propagation distance and normalized modulated amplitude can be seen. The origin for that problem is e.g. the very weak detected signal, SNR is much worse that in measurements using wedges. Also the signal is highly affected

by sound emission from the environment like the machines, acoustic waves from the transmitting transducer, etc. Even isolating the microphone from surrounding noise did not improve the quality of the signal so that it delivered much different results. Nevertheless, the microphone could detect the fundamental frequency components as well as the side bands and higher harmonics of the propagated wave, Figure 49.

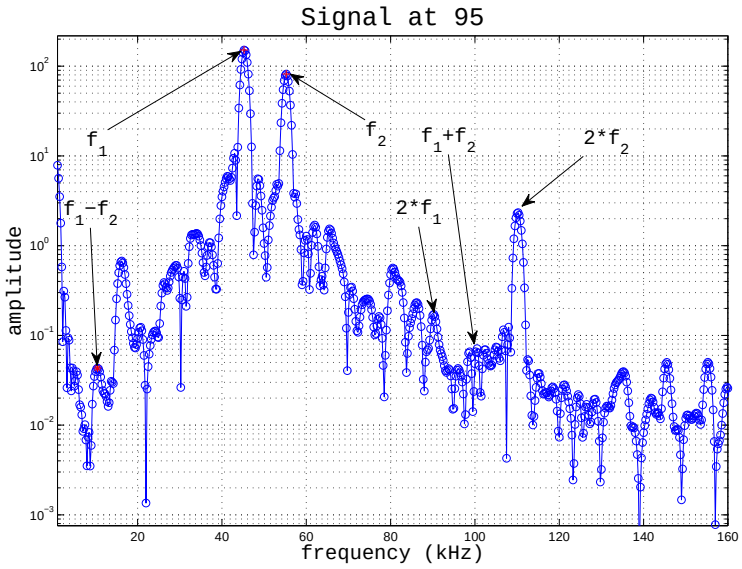

Figure 49: Frequency spectrum of signal received by microphone

.0.2.1 Repeatability

Although the setup was kept the same for all 12 performed measurements using microphone reception on one sample and the distance between the specimen and microphone was controlled in a best possible way, no repeatable results could be achieved. The possible explanations were already mentioned before. The high sensitivity of the microphone to surrounding noise due to its broad band response from $1Hz$ to $10MHz$ overwhelmed the frequencies of interest, which can be well observed in the frequency spectrum Figure 49. Components like $15kHz$ should not appear stronger than the actual difference of fundamental frequencies. This component showed up in every measurement using the microphone, which indicates that this is probably an

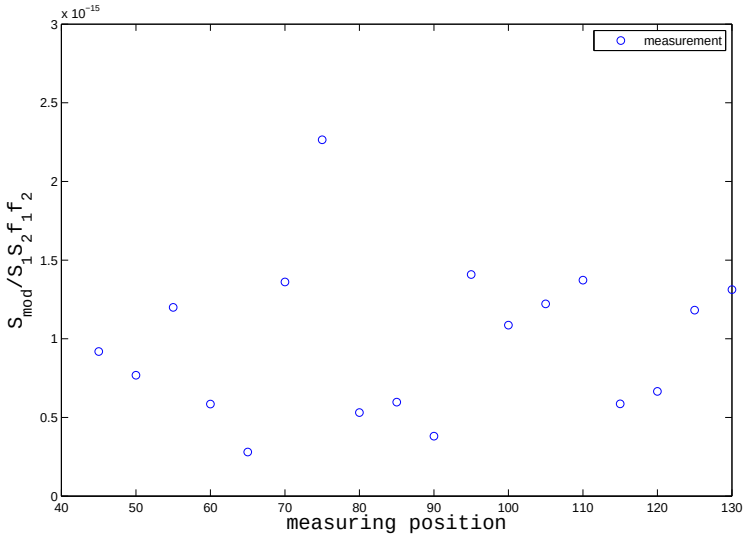

Figure 50: Normalized difference component amplitude over distance

eigen frequency of the devices used. SNR has been much lower than in all other tested methods and the detected signal itself was the weakest. This bears many problems in respect to the signal quality and feasibility of proper frequency spectrum analysis. Furthermore the microphone can be considered as a point receiver, which makes it very sensitive to local effects like change of material properties (matrix and reinforcement materials) and surface inhomogeneities. Especially for concrete it is reasonable to use a signal receiver that are able to average over a finite area to extinguish these effects.

REFERENCES

[1] *Discrete-Time Signal Processing, Third Edition*. Prentice Hall Signal Processing, 2009.

[2] Abeelea, K. E.-A. V. D., Sutin, A., Carmeliet, J., and Johnson, P. A., "Micro-damage diagnostics using nonlinear elastic wave spectroscopy (NEWS)," *NDT&E International*, 2001.

[3] Achenbach, J. D., *Wave Propagation in Elastic Solids*. Elsevier, first ed., 1999.

[4] Antonaci, P., Bruno, C., Gliozzi, A., and Scalerandi, M., "Monitoring evolution of compressive damage in concrete with linear and nonlinear ultrasonic methods," *Cement and Concrete Research*, vol. 40, pp. 1106–1113, 2010.

[5] Armitage, P., Bekers, L., and Wadee, M., "The detection of micro-cracks in concrete by the measurement of ultrasonic harmonic generation and intermodulation,"

[6] Bouchaala, F., C. Payan, V. G., and Balayssac, J., "Carbonation assessment in concrete by nonlinear ultrasound," *Cement and Concrete Research*, vol. 41, pp. 557–559, 2011.

[7] Chen, J., *ULTRA-ACCELERATED ASSESSMENT OF ALKALI-REACTIVITY OF AGGREGATES BY NONLINEAR ACOUSTIC TECHNIQUES*. PhD thesis, Georgia Institute of Technology, 2010.

[8] Daponte, P., Maceri, F., and Olivito, R. S., "Ultrasonic Signal-Processing Techniques for the Measurement of Damage Growth in Structural Materials,"

IEEE TRANSACTIONS ON INSTRUMENTATION AND MEASUREMENT, 1995.

[9] Deroo, F., Kim, J.-Y., Qu, J., Sabra, K., and Jacobs, L. J., "Detection of damage in concrete using diffuse ultrasound (L)," *Acoustical Society of America*, 2010.

[10] Donskoy, D., Sutin, A., and Ekimov, A., "Nonlinear acoustic interaction on contact interfaces and its use for nondestructive testing," *NDT&E International*, vol. 34, pp. 231–238, 2001.

[11] Fabbri, A., Corvisier, J., Schubnel, A., Brunet, F., Goff, B., Rimmele, G., and Barlet-Goudard, V., "Effect of carbonation on the hydro-mechanical properties of Portland cements," *Cement and Concrete Research*, 2009.

[12] Hamilton, M., Il'inskii, Y., and Zabolotskaya, E., "On the existance of stationary nonlinear Rayleigh waves," *Journal of Acousticaal Society of America*, 1993.

[13] Herrmann, J., Kim, J.-Y., Jacobs, L. J., Qu, J., Littles, J. W., and Savage, M. F., "Assessment of material damage in a nickel-base superalloy using nonlinear Rayleigh surface waves," *JOURNAL OF APPLIED PHYSICS*, 2006.

[14] Heusel, R. G., "Experimental Study of the Effects of Concrete Carbonation," tech. rep., School of Civil & Environmental Engineering Georgia Institute of Technology, 2011.

[15] Hu, H., Staszewski, W., Hu, N., Jenal, R., and Qin, G., "Crack detection using nonlinear acoustics and piezoceramic transducers-instantaneous amplitude and frequency analysis," *stacks.iop.org/SMS/19/065017*, 2010.

[16] Kalyanasundaram, N., "Non-linear surface acoustic-waves on an isotropic solid," *International Journal of Engineering Science*, 1981.

[17] Kazakov, V., "A Modulation Crack-Detection Technique: I. Instrumental Method of Implementation," *Russian Journal of Nondestructive Testing*, vol. 31, pp. 709–716, 2006.

[18] Kim, J.-Y., Qu, J., Jacobs, L., Littles, J., and Savage, M., "Acoustic Nonlinearity Parameter Due to Microplasticity," *Journal of Nondestructive Evaluation*, 2006.

[19] Landner, R., "Non-linear surface-waves on an elastic solid," *International Journal of Engineering Science*, 1983.

[20] Leśnicki, K. J., "NONLINEAR RESONANCE METHODS FOR ASSESSING ASR SUSCEPTIBILITY DURING CONCRETE PRISM TESTING (CPT)," Master's thesis, Georgia Institute of Technology, 2011.

[21] Leśnicki, K. J., Kim, J.-Y., Kurtis, K. E., and Jacobs, L. J., "Characterization of ASR damage in concrete using nonlinear impact resonance acoustic spectroscopy technique," *NDT&E International*, 2011.

[22] Liu, M., Tang, G., Jacobs, L. J., and Qu, J., "A NONLINEAR WAVE MIXING METHOD FOR DETECTING ALKALI-SILICA REACTIVITY OF AGGREGATES," , .

[23] Mayer, A., "Surface acoustic-waves in nonlinear elastic media," *Physics Reports-Review Section of Physics Letters*, 1995.

[24] Ngala, V. and Page, C., "EFFECTS OF CARBONATION ON PORE STRUCTURE AND DIFFUSIONAL PROPERTIES OF HYDRATED CEMENT PASTES," *Cement and Concrete Research*, 1997.

[25] Payan, C., Garnier, V., and Moysan, J., "Applying nonlinear resonant ultrasound spectroscopy to improving thermal damage assessment in concrete," *JASA Express Letters*, 2007.

[26] Saetta, A. V., Schrefler, B. A., and Vitaliani, R. V., "THE CARBONATION OF CONCRETE AND THE MECHANISM OF MOISTURE, HEAT AND CARBON DIOXIDE FLOW THROUGH POROUS MATERIALS," *CEMENT and CONCRETE RESEARCH*, vol. 23, pp. 761–772, 1993.

[27] Saettaa, A. V. and Vitaliani, R. V., "Experimental investigation and numerical modeling of carbonation process in reinforced concrete structures Part II. Practical applications," *Cement and Concrete Research*, 2005.

[28] Sargolzahi, M., Kodjo, S. A., Rivard, P., and Rhazi, J., "Effectiveness of nondestructive testing for the evaluation of alkalisilica reaction in concrete," *Construction and Building Materials*, vol. 24, pp. 1398–1403, 2010.

[29] Schurr, D. P., Kim, J.-Y., Sabra, K. G., and Jacobs, L. J., "Damage detection in concrete using coda wave interferometry," *NDT&E International*, 2011.

[30] Shah, A. and Ribakov, Y., "Non-linear ultrasonic evaluation of damaged concrete based on higher order harmonic generation," *Materials and Design*, 2009.

[31] Solodov, I., Wackerl, J., Pfleiderer, K., and Busse, G., "Nonlinear self-modulation and subharmonic acoustic spectroscopy for damage detection and location," *APPLIED PHYSICS LETTERS*, vol. 84, no. 26, 2006.

[32] Walker, S., "CHARACTERIZATION OF FATIGUE DAMAGE IN A36 STEEL SPECIMENS USING NONLINEAR RAYLEIGH SURFACE WAVES," Master's thesis, Georgia Institute of Technology, 2011.

[33] Warnemuende, K. and Wu, H.-C., "Actively modulated acoustic nondestructive evaluation of concrete," *Cement and Concrete Research*, vol. 34, pp. 563–570, 2004.

REFERENCES

[1] *Discrete-Time Signal Processing, Third Edition*. Prentice Hall Signal Processing, 2009.

[2] Abeelea, K. E.-A. V. D., Sutin, A., Carmeliet, J., and Johnson, P. A., "Micro-damage diagnostics using nonlinear elastic wave spectroscopy (NEWS)," *NDT&E International*, 2001.

[3] Achenbach, J. D., *Wave Propagation in Elastic Solids*. Elsevier, first ed., 1999.

[4] Antonaci, P., Bruno, C., Gliozzi, A., and Scalerandi, M., "Monitoring evolution of compressive damage in concrete with linear and nonlinear ultrasonic methods," *Cement and Concrete Research*, vol. 40, pp. 1106–1113, 2010.

[5] Armitage, P., Bekers, L., and Wadee, M., "The detection of micro-cracks in concrete by the measurement of ultrasonic harmonic generation and intermodulation,"

[6] Bouchaala, F., C. Payan, V. G., and Balayssac, J., "Carbonation assessment in concrete by nonlinear ultrasound," *Cement and Concrete Research*, vol. 41, pp. 557–559, 2011.

[7] Chen, J., *ULTRA-ACCELERATED ASSESSMENT OF ALKALI-REACTIVITY OF AGGREGATES BY NONLINEAR ACOUSTIC TECHNIQUES*. PhD thesis, Georgia Institute of Technology, 2010.

[8] Daponte, P., Maceri, F., and Olivito, R. S., "Ultrasonic Signal-Processing Techniques for the Measurement of Damage Growth in Structural Materials," *IEEE TRANSACTIONS ON INSTRUMENTATION AND MEASUREMENT*, 1995.

[9] Deroo, F., Kim, J.-Y., Qu, J., Sabra, K., and Jacobs, L. J., "Detection of damage in concrete using diffuse ultrasound (L)," *Acoustical Society of America*, 2010.

[10] Donskoy, D., Sutin, A., and Ekimov, A., "Nonlinear acoustic interaction on contact interfaces and its use for nondestructive testing," *NDT&E International*, vol. 34, pp. 231–238, 2001.

[11] Fabbri, A., Corvisier, J., Schubnel, A., Brunet, F., Goff, B., Rimmele, G., and Barlet-Goudard, V., "Effect of carbonation on the hydromechanical properties of Portland cements," *Cement and Concrete Research*, 2009.

[12] Hamilton, M., Il'inskii, Y., and Zabolotskaya, E., "On the existance of stationary nonlinear Rayleigh waves," *Journal of Acousticaal Society of America*, 1993.

[13] Herrmann, J., Kim, J.-Y., Jacobs, L. J., Qu, J., Littles, J. W., and Savage, M. F., "Assessment of material damage in a nickel-base superalloy using nonlinear Rayleigh surface waves," *JOURNAL OF APPLIED PHYSICS*, 2006.

[14] Heusel, R. G., "Experimental Study of the Effects of Concrete Carbonation," tech. rep., School of Civil & Environmental Engineering Georgia Institute of Technology, 2011.

[15] Hu, H., Staszewski, W., Hu, N., Jenal, R., and Qin, G., "Crack detection using nonlinear acoustics and piezoceramic transducers-instantaneous amplitude and frequency analysis," *stacks.iop.org/SMS/19/065017*, 2010.

[16] Kalyanasundaram, N., "Non-linear surface acoustic-waves on an isotropic solid," *International Journal of Engineering Science*, 1981.

[17] Kazakov, V., "A Modulation Crack-Detection Technique: I. Instrumental Method of Implementation," *Russian Journal of Nondestructive Testing*, vol. 31, pp. 709–716, 2006.

[18] Kim, J.-Y., Qu, J., Jacobs, L., Littles, J., and Savage, M., "Acoustic Nonlinearity Parameter Due to Microplasticity," *Journal of Nondestructive Evaluation*, 2006.

[19] Landner, R., "Non-linear surface-waves on an elastic solid," *International Journal of Engineering Science*, 1983.

[20] Leśnicki, K. J., "NONLINEAR RESONANCE METHODS FOR ASSESSING ASR SUSCEPTIBILITY DURING CONCRETE PRISM TESTING (CPT)," Master's thesis, Georgia Institute of Technology, 2011.

[21] Leśnicki, K. J., Kim, J.-Y., Kurtis, K. E., and Jacobs, L. J., "Characterization of ASR damage in concrete using nonlinear impact resonance acoustic spectroscopy technique," *NDT&E International*, 2011.

[22] Liu, M., Tang, G., Jacobs, L. J., and Qu, J., "A NONLINEAR WAVE MIXING METHOD FOR DETECTING ALKALI-SILICA REACTIVITY OF AGGREGATES," , .

[23] Mayer, A., "Surface acoustic-waves in nonlinear elastic media," *Physics Reports-Review Section of Physics Letters*, 1995.

[24] Ngala, V. and Page, C., "EFFECTS OF CARBONATION ON PORE STRUCTURE AND DIFFUSIONAL PROPERTIES OF HYDRATED CEMENT PASTES," *Cement and Concrete Research*, 1997.

[25] Payan, C., Garnier, V., and Moysan, J., "Applying nonlinear resonant ultrasound spectroscopy to improving thermal damage assessment in concrete," *JASA Express Letters*, 2007.

[26] Saetta, A. V., Schrefler, B. A., and Vitaliani, R. V., "THE CARBONATION OF CONCRETE AND THE MECHANISM OF MOISTURE, HEAT AND CARBON DIOXIDE FLOW THROUGH POROUS MATERIALS," *CEMENT and CONCRETE RESEARCH*, vol. 23, pp. 761–772, 1993.

[27] Saettaa, A. V. and Vitaliani, R. V., "Experimental investigation and numerical modeling of carbonation process in reinforced concrete structures Part II. Practical applications," *Cement and Concrete Research*, 2005.

[28] Sargolzahi, M., Kodjo, S. A., Rivard, P., and Rhazi, J., "Effectiveness of nondestructive testing for the evaluation of alkalisilica reaction in concrete," *Construction and Building Materials*, vol. 24, pp. 1398–1403, 2010.

[29] Schurr, D. P., Kim, J.-Y., Sabra, K. G., and Jacobs, L. J., "Damage detection in concrete using coda wave interferometry," *NDT&E International*, 2011.

[30] Shah, A. and Ribakov, Y., "Non-linear ultrasonic evaluation of damaged concrete based on higher order harmonic generation," *Materials and Design*, 2009.

[31] Solodov, I., Wackerl, J., Pfleiderer, K., and Busse, G., "Nonlinear self-modulation and subharmonic acoustic spectroscopy for damage detection and location," *APPLIED PHYSICS LETTERS*, vol. 84, no. 26, 2006.

[32] Walker, S., "CHARACTERIZATION OF FATIGUE DAMAGE IN A36 STEEL SPECIMENS USING NONLINEAR RAYLEIGH SURFACE WAVES," Master's thesis, Georgia Institute of Technology, 2011.

[33] Warnemuende, K. and Wu, H.-C., "Actively modulated acoustic nondestructive evaluation of concrete," *Cement and Concrete Research*, vol. 34, pp. 563–570, 2004.